

Study of Conical Intersections and Non-adiabatic effects for HeH_2^+ molecular ion

Ankur Kumar Gupta

*A dissertation submitted for the partial fulfilment of
BS-MS dual degree in Science*



Indian Institute of Science Education and Research Mohali
April 2015

Certificate of Examination

This is to certify that the dissertation titled “**Study of Conical Intersections and Non-adiabatic effects for HeH_2^+ molecular ion**” submitted by **Mr. Ankur Kumar Gupta** (Reg. No. MS10056) for the partial fulfilment of BS-MS dual degree programme of the Institute, has been examined by the thesis committee duly appointed by the Institute. The committee finds the work done by the candidate satisfactory and recommends that the report be accepted.

Dr. P. Balanarayan

Dr. K. R. Shamasundar

Professor N. Sathyamurthy
(Supervisor)

Dated: April 24, 2015

Declaration

The work presented in this dissertation has been carried out by me under the guidance of Professor N. Sathyamurthy at the Indian Institute of Science Education and Research Mohali.

This work has not been submitted in part or in full for a degree, a diploma, or a fellowship to any other university or institute. Whenever contributions of others are involved, every effort is made to indicate this clearly, with due acknowledgement of collaborative research and discussions. This thesis is a bonafide record of original work done by me and all sources listed within have been detailed in the bibliography.

Ankur Kumar Gupta
(Candidate)

Dated: April 24, 2015

In my capacity as the supervisor of the candidate's project work, I certify that the above statements by the candidate are true to the best of my knowledge.

Professor N. Sathyamurthy
(Supervisor)

Acknowledgement

I would like to take this opportunity to convey my gratitude to

- Professor N. Sathyamurthy for guiding my master's thesis project. I find myself fortunate to have an opportunity to work under a teacher having genius level intellect and vast academic experience.
- Professor M. Baer for introducing me to the subject on which the present study is based. His enthusiasm about his field encouraged me to work harder.
- Vikash Dhindhwal, Satyam Ravi, and Dr. Saurabh Srivastava for patiently answering my silly doubts and involving in many fruitful discussions.
- Computer Center, IISER Mohali for allowing me to use the facilities without which I wouldn't have been able to get any of the results.
- Upakul Sarma for keeping the lab environment lively.
- all Chemistry faculty for being great teachers.
- my friends in IISER Mohali and elsewhere for being there for me.
- my parents and sister for always supporting me.
- my younger brother Krishna, my joy and source of strength.

Ankur Kumar Gupta
MS10056
IISER Mohali

List of Figures

1.1	Section of (a) Renner-Teller CI and (b) a general or Jahn-Teller CI. ¹³ . . .	15
2.1	HeH ₂ ⁺ molecule with a closed contour (in red) in nuclear configuration space	18
2.2	Linear HeH ₂ ⁺ molecule	19
2.3	PES diagram depicting the lowest three states for linear HeH ₂ ⁺	20
2.4	Close-up view of the region where the PESs of the two lowest excited states are close to each other (for linear HeH ₂ ⁺)	21
2.5	Molecular configuration of HeH ₂ ⁺ used to calculate NACTs and ADT angle	21
2.6	Plots of NACTs, ADT angle, and energy as a function of ϕ for $q = 0.1\text{\AA}$ of Scheme-1	24
2.7	Plots of NACTs, ADT angle, and energy as a function of ϕ for $q = 0.2\text{\AA}$ of Scheme-1	25
2.8	Plots of NACTs, ADT angle, and energy as a function of ϕ for $q = 0.3\text{\AA}$ of Scheme-1	26
2.9	Plots of NACTs, ADT angle, and energy as a function of ϕ for $q = 0.4\text{\AA}$ of Scheme-1	27
2.10	Plots of NACTs, ADT angle, and energy as a function of ϕ for $q = 0.6\text{\AA}$ of Scheme-1	28
2.11	Plots of NACTs, and energy as a function of ϕ for $q = 1.0\text{\AA}$ of Scheme-1	29
2.12	Plots of NACTs, and energy as a function of ϕ for $q = 1.3\text{\AA}$ of Scheme-1	30
2.13	Plots of NACTs, and energy as a function of ϕ for $q = 1.5\text{\AA}$ of Scheme-1	31
2.14	Special case: Plots of NACTs, ADT angle, and energy as a function of ϕ for $q = 1.8\text{\AA}$ of Scheme-1	32
2.15	Plots of NACTs, ADT angle, and energy as a function of ϕ for $q = 0.1\text{\AA}$ of Scheme-2	34

2.16	Plots of NACTs, ADT angle, and energy as a function of ϕ for $q = 0.2\text{\AA}$ of Scheme-2	35
2.17	Plots of NACTs, ADT angle, and energy as a function of ϕ for $q = 0.3\text{\AA}$ of Scheme-2	36
2.18	Plots of NACTs, ADT angle, and energy as a function of ϕ for $q = 0.4\text{\AA}$ of Scheme-2	37
2.19	Plots of NACTs, ADT angle, and energy as a function of ϕ for $q = 0.6\text{\AA}$ of Scheme-2	38
2.20	Plots of NACTs, ADT angle, and energy as a function of ϕ for $q = 1.0\text{\AA}$ of Scheme-2	39
2.21	Plots of NACTs, ADT angle, and energy as a function of ϕ for $q = 1.2\text{\AA}$ of Scheme-2	40
2.22	Plots of NACTs, ADT angle, and energy as a function of ϕ for $q = 1.8\text{\AA}$ of Scheme-2	41
2.23	Non-linear HHeH ⁺ molecule	42
2.24	PES diagram depicting lowest three states for non-linear HHeH ⁺	43
2.25	Close-up view of the region where the PESs of the two lowest electronic states are close to each other (for non-linear HHeH ⁺)	44
2.26	Molecular configuration of HHeH ⁺ used to calculate NACTs and ADT angle	44
2.27	Molecular configuration of non-linear HHeH ⁺ at which (1,2) CI is observed	46
2.28	Plots of NACTs, ADT angle, and energy as a function of ϕ for $q = 0.1\text{\AA}$ for non-linear HHeH ⁺	47
2.29	Plots of NACTs, ADT angle, and energy as a function of ϕ for $q = 0.2\text{\AA}$ for non-linear HHeH ⁺	48
2.30	Plots of NACTs, ADT angle, and energy as a function of ϕ for $q = 0.3\text{\AA}$ for non-linear HHeH ⁺	49
2.31	Plots of NACTs, ADT angle, and energy as a function of ϕ for $q = 0.4\text{\AA}$ for non-linear HHeH ⁺	50
2.32	Plots of NACTs, ADT angle, and energy as a function of ϕ for $q = 0.6\text{\AA}$ for non-linear HHeH ⁺	51
2.33	Plots of NACTs, ADT angle, and energy as a function of ϕ for $q = 0.8\text{\AA}$ for non-linear HHeH ⁺	52
2.34	Plots of NACTs, ADT angle, and energy as a function of ϕ for $q = 1.2\text{\AA}$ for non-linear HHeH ⁺	53

2.35	Plots of NACTs, ADT angle, and energy as a function of ϕ for $q = 1.6\text{\AA}$ for non-linear HHeH ⁺	54
2.36	Plots of NACTs, ADT angle, and energy as a function of ϕ for $q = 2.0\text{\AA}$ for non-linear HHeH ⁺	55

Acronyms

ADT	Adiabatic-to-Diabatic Transformation
JT CI	Jahn-Teller Conical Intersection
RT CI	Renner-Teller Conical Intersection
NACT	Non-Adiabatic Coupling Term
PEC	Potential Energy Curve
PES	Potential Energy Surface
CI	Conical Intersection

Contents

List of Figures	iv
Acronyms	v
Contents	vi
Abstract	vii
1 Introduction to Non-adiabatic Coupling and Conical Intersections	1
1.1 Introduction	1
1.2 Coupling between Nuclear and Electronic motion	2
1.2.1 Non-adiabatic Coupling	3
1.2.2 Vibronic Coupling	5
1.3 Adiabatic-to-Diabatic Transformation (ADT)	7
1.4 π Quantization Condition	9
1.4.1 3-state Calculation	10
1.5 Potential Energy Surfaces (PESs)	12
1.6 Non-adiabatic Processes and Conical Intersections (CIs)	12
2 Results & Discussion	17
2.1 Computational Details	17
2.2 Linear HeH_2^+	19
2.2.1 Scheme-1	22
2.2.2 Scheme-2	33
2.3 Non-linear HHeH^+	42
2.4 Conclusion	56
Bibliography	57

Abstract

HeH_2^+ has been the subject of much research for the past 4-5 decades. We are interested in studying the *potential energy surfaces* and locating the associated *conical intersections* for this molecular system. Therefore, it is imperative to have a thorough understanding of the coupling between electronic and nuclear motion and conical intersections which we have explained in detail in Chapter 1. One of the most important properties of conical intersections is that they show *geometric phase effect* (sign flip of electronic wavefunctions) which we have used to our advantage to derive conditions to confirm the presence of an intersection between potential energy surfaces. We then applied this theory to HeH_2^+ and obtained the corresponding results which we have discussed in Chapter 2.

Chapter 1

Introduction to Non-adiabatic Coupling and Conical Intersections

1.1 Introduction

Hydrogen (H) and Helium (He) are the two most abundant elements in the universe, making up almost 99% of its mass. These two elements are involved in most of the reactions happening in stars and the interstellar medium. Naturally, many molecular species comprising only H and He have been the subject of much research. But the molecule garnering the most interest in the scientific fraternity is HeH_2^+ , and not only due to its significance in the field of Astrochemistry. HeH_2^+ , a very simple ion-molecule system, is one of the most studied molecular systems, both experimentally and theoretically. It was the first molecular system for which vibrational enhancement was observed, experimentally.¹ And theoretically for the first time, reactive scattering resonances were predicted using quantum mechanical calculations.² But many inconsistencies between theory and experimental observation have been reported for HeH_2^+ , and this is also one of the reasons that the scientific literature is full of research for HeH_2^+ . So, taking a step in the direction to understand this troublesome molecule in a more better way, we have dedicated the present study to investigate the PESs (potential for nuclear motion, more in Section 1.5) of linear HeH_2^+ and confirm the location of CIs (formed when two or more PESs intersect, see more in Section 1.6) formed by them. At CIs, the PESs are in close proximity due to which the nuclear motion is no longer constrained to a single PES resulting in a strong coupling between nuclear and electronic motion. So, before moving on to tackle the HeH_2^+ molecule, we intend to understand the theory on which the present study is

based.

1.2 Coupling between Nuclear and Electronic motion

We would like to see how nuclear and electronic motion are coupled to each other. In this section, we will derive some mathematical relations which reveal this coupling.

The total Hamiltonian of a molecule, neglecting spin-orbit coupling and other relativistic effects can be written as,

$$\mathbf{H}(\mathbf{r}, \mathbf{R}) = T_n(\mathbf{R}) + T_e(\mathbf{r}) + U(\mathbf{r}, \mathbf{R}), \quad (1.1)$$

where

$$U(\mathbf{r}, \mathbf{R}) = U_{ee}(\mathbf{r}) + U_{ne}(\mathbf{r}, \mathbf{R}) + U_{nn}(\mathbf{R}). \quad (1.2)$$

\mathbf{r} and \mathbf{R} represent electronic and nuclear coordinates, respectively. T_n and T_e in equation (1.1) are representing nuclear kinetic energy operator and electronic kinetic energy operator, respectively. U is the potential energy term which includes electron-electron repulsion (U_{ee}), electron-nuclear attraction (U_{ne}), and nuclear-nuclear repulsion (U_{nn}) terms, given by equation (1.2).

The time-independent Schrödinger equation for a molecule can be written as,

$$(\mathbf{H}(\mathbf{r}, \mathbf{R}) - \varepsilon)\Psi(\mathbf{r}, \mathbf{R}) = 0 \quad (1.3)$$

where, ε is the total energy and $\Psi(\mathbf{r}, \mathbf{R})$ represents the total wavefunction of the molecule.

Solving equation (1.3) without making any approximations is almost an impossible task. So, we will make use of the *Born-Oppenheimer approximation* which encourages to solve the Schrödinger equation for the electrons in the static electric potential resulting from the nuclei in a fixed configuration. This approximation is based on the huge mass difference between electrons and nuclei due to which the electrons can react immediately to any (small) change in the nuclear configuration. Equipped with this approximation, we will solve the total time-independent Schrödinger equation using two different approaches and see how the coupling between nuclear and electronic motion arises mathematically in these two cases.

1.2.1 Non-adiabatic Coupling

Within the framework of Born-Oppenheimer approximation, the *adiabatic* representation of the total wavefunction of a molecule can be written as,

$$\Psi(\mathbf{r}, \mathbf{R}) = \sum_j \chi_j(\mathbf{R}) \phi_j(\mathbf{r}; \mathbf{R}) \quad (1.4)$$

where $\chi_j(\mathbf{R})$ are the nuclear wavefunctions, and $\phi_j(\mathbf{r}; \mathbf{R})$ are the *adiabatic* electronic wavefunctions and they depend parametrically on nuclear coordinates.

The electronic wavefunctions ($\phi_j(\mathbf{r}; \mathbf{R})$) are eigenfunctions of electronic Hamiltonian ($H_e(\mathbf{r}; \mathbf{R})$) and the equation which relates these two entities is the time-independent Schrödinger equation for electronic motion:

$$(H_e(\mathbf{r}; \mathbf{R}) - E_j(\mathbf{R})) \phi_j(\mathbf{r}; \mathbf{R}) = 0 \quad (1.5)$$

where

$$H_e(\mathbf{r}; \mathbf{R}) = T_e(\mathbf{r}) + U(\mathbf{r}, \mathbf{R}) \quad (1.6)$$

and $E_j(\mathbf{R})$ is the electronic energy (including internuclear repulsion) of the j^{th} state.

Substituting equation (1.4) in equation (1.3), and using equations (1.5) and (1.6), we obtain

$$\sum_j T_n(\mathbf{R}) \chi_j(\mathbf{R}) \phi_j(\mathbf{r}; \mathbf{R}) + \sum_j E_j(\mathbf{R}) \chi_j(\mathbf{R}) \phi_j(\mathbf{r}; \mathbf{R}) - \varepsilon \sum_j \chi_j(\mathbf{R}) \phi_j(\mathbf{r}; \mathbf{R}) = 0 \quad (1.7)$$

The nuclear kinetic energy operator (in terms of mass scaled coordinates) is written as,^{3,4}

$$T_n(\mathbf{R}) = -\frac{\hbar^2}{2m} \nabla^2 \quad (1.8)$$

where m represents mass of the system.

Substituting equation (1.8) in equation (1.7), left multiplying equation (1.7) by $\phi_i^*(\mathbf{r}; \mathbf{R})$, and then integrating with respect to electronic coordinates gives us

$$-\frac{\hbar^2}{2m} \nabla^2 \chi_i + (E_i - \varepsilon) \chi_i - \frac{\hbar^2}{2m} \sum_j (2\tau_{ij} \cdot \nabla + \tau_{ij}^{(2)}) \chi_j = 0, \quad (1.9)$$

Equation (1.9) can be written in matrix form as,

$$-\frac{\hbar^2}{2m} \nabla^2 \boldsymbol{\chi} + (\mathbf{E} - \varepsilon) \boldsymbol{\chi} - \frac{\hbar^2}{2m} (2\boldsymbol{\tau} \cdot \nabla + \boldsymbol{\tau}^{(2)}) \boldsymbol{\chi} = 0, \quad (1.10)$$

where $\boldsymbol{\chi}(\mathbf{R})$ is a column matrix containing the nuclear wavefunctions and \mathbf{E} is a diagonal matrix containing the adiabatic electronic energy.

$\boldsymbol{\tau}$ and $\boldsymbol{\tau}^{(2)}$ in equation (1.10) are matrices containing the **Non-Adiabatic Coupling Terms (NACTs)**.⁴ $\boldsymbol{\tau}$ is called the first-order non-adiabatic coupling matrix. It is a vector matrix since each of its elements is a vector and is given as,

$$\tau_{ij}(\mathbf{R}) = \langle \phi_i(\mathbf{r}; \mathbf{R}) | \nabla \phi_j(\mathbf{r}; \mathbf{R}) \rangle \quad (1.11)$$

$\boldsymbol{\tau}^{(2)}$ is known as the second-order non-adiabatic coupling matrix, which is a scalar matrix with matrix elements having the following form,

$$\tau_{ij}^{(2)}(\mathbf{R}) = \langle \phi_i(\mathbf{r}; \mathbf{R}) | \nabla^2 \phi_j(\mathbf{r}; \mathbf{R}) \rangle \quad (1.12)$$

As can be seen from the form of equations (1.11) and (1.12), NACTs couple nuclear and electronic components and also different electronic states.

We will now derive an equation which connects NACTs with the energy of the corresponding states. To do that, we consider equation (1.5) which is the electronic time-independent Schrödinger equation. We differentiate this equation with respect to the nuclear coordinates to get,

$$\begin{aligned} (\nabla H_e(\mathbf{r}; \mathbf{R}) | \phi_j(\mathbf{r}; \mathbf{R}) \rangle + H_e(\mathbf{r}; \mathbf{R}) (\nabla | \phi_j(\mathbf{r}; \mathbf{R}) \rangle) - (\nabla E_j(\mathbf{R}) | \phi_j(\mathbf{r}; \mathbf{R}) \rangle \\ - E_j(\mathbf{R}) (\nabla | \phi_j(\mathbf{r}; \mathbf{R}) \rangle) = 0 \end{aligned} \quad (1.13)$$

Left multiplying equation (1.13) by $\langle \phi_i(\mathbf{r}; \mathbf{R}) |$ ($i \neq j$) and then integrating over electronic coordinates gives us,

$$\begin{aligned} \langle \phi_i(\mathbf{r}; \mathbf{R}) | \nabla H_e(\mathbf{r}; \mathbf{R}) | \phi_j(\mathbf{r}; \mathbf{R}) \rangle + \langle \phi_i(\mathbf{r}; \mathbf{R}) | H_e(\mathbf{r}; \mathbf{R}) | \nabla \phi_j(\mathbf{r}; \mathbf{R}) \rangle \\ - E_j(\mathbf{R}) \langle \phi_i(\mathbf{r}; \mathbf{R}) | \nabla \phi_j(\mathbf{r}; \mathbf{R}) \rangle = 0 \end{aligned} \quad (1.14)$$

The third term in equation (1.13) became zero because the electronic wavefunctions are orthogonal in nature.

We know that the Hamiltonian operator can act on a *bra* state in the following manner,

$$\langle \phi_j(\mathbf{r}; \mathbf{R}) | H_e(\mathbf{r}; \mathbf{R}) - \langle \phi_j(\mathbf{r}; \mathbf{R}) | E_j(\mathbf{R}) = 0 \quad (1.15)$$

Using equations (1.11) and (1.15), we can rewrite equation (1.14) as,

$$\langle \phi_i(\mathbf{r}; \mathbf{R}) | \nabla H_e(\mathbf{r}; \mathbf{R}) | \phi_j(\mathbf{r}; \mathbf{R}) \rangle + E_i(\mathbf{r}; \mathbf{R}) \tau_{ij} - E_j(\mathbf{r}; \mathbf{R}) \tau_{ij} = 0 \quad (1.16)$$

Rearranging equation (1.16) a bit gives the desired equation for NACT,

$$\tau_{ij} = \frac{\langle \phi_i(\mathbf{r}; \mathbf{R}) | \nabla H_e(\mathbf{r}; \mathbf{R}) | \phi_j(\mathbf{r}; \mathbf{R}) \rangle}{E_j(\mathbf{r}; \mathbf{R}) - E_i(\mathbf{r}; \mathbf{R})} \quad (1.17)$$

It is clear from equation (1.17) that the magnitude of NACT for a pair of states is inversely proportional to the energy difference between them. As the PESs come close to each other, the magnitude of NACTs increases and at the point of degeneracy, the two energies become equal which implies NACT is not defined at that point since the denominator in equation (1.17) is zero in such a case. This is why it is of utmost importance to consider NACTs whenever we are dealing with processes which depend on the close proximity of PESs.

Some other important properties of NACTs which we are stating without proof, are,

$$\tau_{ij}(\mathbf{R}) = -\tau_{ji}(\mathbf{R}) \quad (1.18)$$

$$\tau_{ii}(\mathbf{R}) = 0 \quad (1.19)$$

provided the electronic wavefunctions are assumed to be real.

1.2.2 Vibronic Coupling

Let's assume that, initially the molecule is in electronic state R at some *reference* nuclear configuration \mathbf{R}_0 . Now, suppose the state of the molecule changes from R to S . Due to this electronic transition (change of state), there is relocation of electronic charge which changes the Coulombic force acting on the nuclei and this results in change of nuclear configuration from \mathbf{R}_0 to \mathbf{R} .⁵ And if $\Delta\mathbf{R} = \mathbf{R} - \mathbf{R}_0$ is small, then we can expand the potential energy term ($U(\mathbf{r}, \mathbf{R})$) in equation (1.1) using the Taylor series around the *reference* configuration \mathbf{R}_0 as,

$$\begin{aligned} H(\mathbf{r}, \mathbf{Q}) = T_n(\mathbf{Q}) + T_e(\mathbf{r}) + U(\mathbf{r}, \mathbf{R}_0) + \sum_{\alpha} \left(\frac{\partial U}{\partial Q_{\alpha}} \right)_{\mathbf{R}_0} Q_{\alpha} \\ + \frac{1}{2} \sum_{\alpha} \sum_{\beta} \left(\frac{\partial^2 U}{\partial Q_{\alpha} \partial Q_{\beta}} \right)_{\mathbf{R}_0} Q_{\alpha} Q_{\beta} + \dots \end{aligned} \quad (1.20)$$

where \mathbf{Q} refers to the normal coordinates for the nuclei. The above equation is also called *Herzberg-Teller expansion*.

Making use of the above discussion, we can write the total wavefunction of the molecule in a slightly different way from equation (1.4) as,

$$\Psi(\mathbf{r}, \mathbf{Q}) = \sum_j \chi_j(\mathbf{Q}) \phi_j(\mathbf{r}; \mathbf{R}_0) \quad (1.21)$$

where we have used the *adiabatic* electronic wavefunctions ($\phi_j(\mathbf{r}; \mathbf{R}_0)$). Hence, equation (1.21) is called the *adiabatic* representation of the total wavefunction.

In such a case the time-independent Schrödinger equation can be written as

$$(H_e(\mathbf{r}; \mathbf{R}_0) - E_j(\mathbf{R}_0))\phi_j(\mathbf{r}; \mathbf{R}_0) = 0 \quad (1.22)$$

where

$$H_e(\mathbf{r}; \mathbf{R}_0) = T_e(\mathbf{r}) + U(\mathbf{r}, \mathbf{R}_0) \quad (1.23)$$

and $E_j(\mathbf{R}_0)$ is the electronic energy of the j^{th} state at the *reference* nuclear configuration \mathbf{R}_0 .

If we substitute equations (1.20) and (1.21) in (1.3), make use of equation (1.22), and then simplify, we obtain

$$\begin{aligned} \sum_j \phi_j(\mathbf{r}; \mathbf{R}_0) T_n(\mathbf{Q}) \chi_j(\mathbf{Q}) + \sum_j \Delta U \chi_j(\mathbf{Q}) \phi_j(\mathbf{r}; \mathbf{R}_0) + \sum_j E_j(\mathbf{R}_0) \chi_j(\mathbf{Q}) \phi_j(\mathbf{r}; \mathbf{R}_0) \\ - \varepsilon \sum_j \chi_j(\mathbf{Q}) \phi_j(\mathbf{r}; \mathbf{R}_0) = 0 \end{aligned} \quad (1.24)$$

where

$$\Delta U = \sum_{\alpha} \left(\frac{\partial U}{\partial Q_{\alpha}} \right)_{\mathbf{R}_0} Q_{\alpha} + \frac{1}{2} \sum_{\alpha} \sum_{\beta} \left(\frac{\partial^2 U}{\partial Q_{\alpha} \partial Q_{\beta}} \right)_{\mathbf{R}_0} Q_{\alpha} Q_{\beta} + \dots \quad (1.25)$$

Now, if we left multiply equation (1.24) by $\phi_i^*(\mathbf{r}; \mathbf{R}_0)$ and then integrate it over the electronic coordinates, we obtain

$$\begin{aligned} \left(T_n(\mathbf{Q}) + E_i(\mathbf{R}_0) - \varepsilon + \sum_{\alpha} (V_{\alpha})_{ii} Q_{\alpha} + \frac{1}{2} \sum_{\alpha, \beta} (W_{\alpha\beta})_{ii} Q_{\alpha} Q_{\beta} + \dots \right) \chi_i(\mathbf{Q}) \\ + \sum_{j \neq i} \left(\sum_{\alpha} (V_{\alpha})_{ij} Q_{\alpha} + \frac{1}{2} \sum_{\alpha, \beta} (W_{\alpha\beta})_{ij} Q_{\alpha} Q_{\beta} + \dots \right) \chi_j(\mathbf{Q}) = 0 \end{aligned} \quad (1.26)$$

where

$$(V_{\alpha})_{ij} = \left\langle \phi_i(\mathbf{r}; \mathbf{R}_0) \left| \left(\frac{\partial U}{\partial Q_{\alpha}} \right)_{\mathbf{R}_0} \right| \phi_j(\mathbf{r}; \mathbf{R}_0) \right\rangle \quad (1.27)$$

$$(W_{\alpha\beta})_{ij} = \left\langle \phi_i(\mathbf{r}; \mathbf{R}_0) \left| \left(\frac{\partial^2 U}{\partial Q_{\alpha} \partial Q_{\beta}} \right)_{\mathbf{R}_0} \right| \phi_j(\mathbf{r}; \mathbf{R}_0) \right\rangle \quad (1.28)$$

and they are known as linear and quadratic **Vibronic Coupling Terms (VCTs)**,⁶ respectively. The mathematical form of VCTs (like NACTs) indicates coupling between nuclear and electronic motion and also between different electronic states.

1.3 Adiabatic-to-Diabatic Transformation (ADT)

In this section, we will see how *adiabatic* and *diabatic* representations are related to each other and we will use this relation to derive quantitative conditions to confirm the presence of CIs (section 1.6) between two PESs (section 1.5).

The *adiabatic* and *diabatic* electronic wavefunctions, $\phi(\mathbf{r}; \mathbf{R})$ and $\phi(\mathbf{r}; \mathbf{R}_0)$ respectively, are connected by an orthogonal transformation,

$$\phi(\mathbf{r}; \mathbf{R}) = \mathbf{A}(\mathbf{R})\phi(\mathbf{r}; \mathbf{R}_0) \quad (1.29)$$

where, \mathbf{A} is an orthogonal matrix and is called the **ADT matrix**.

We have assumed that the electronic wavefunctions $\phi_j(\mathbf{r}; \mathbf{R}); j = 1, 2, \dots, N$ form a complete basis set in an N-dimensional *Hilbert space*. Now, $|\nabla\phi_j\rangle$ (∇ is derivative with respect to nuclear coordinates) is a function of electronic coordinates and exist in the same Hilbert space, thus it can be expanded as a linear combination of electronic wavefunctions as,

$$\nabla |\phi_j(\mathbf{r}; \mathbf{R})\rangle = \sum_{k=1}^N z_{jk} |\phi_k(\mathbf{r}; \mathbf{R})\rangle \quad (1.30)$$

Left multiplying both sides of the equation (1.30) by $\langle\phi_i(\mathbf{r}; \mathbf{R})|$ and then integrating over electronic coordinates gives us,

$$\langle\phi_i(\mathbf{r}; \mathbf{R})|\nabla\phi_j(\mathbf{r}; \mathbf{R})\rangle = z_{ji} \quad (1.31)$$

where we have used the orthogonality property of the electronic wavefunctions to obtain equation (1.31). The LHS of equation (1.31) is nothing but the NACT ($\tau_{ij}(\mathbf{R})$). So, using equations (1.31) and (1.18), we can rewrite equation (1.30) as,

$$\nabla |\phi_j(\mathbf{r}; \mathbf{R})\rangle = - \sum_{k=1}^N \tau_{jk}(\mathbf{R}) |\phi_k(\mathbf{r}; \mathbf{R})\rangle \quad (1.32)$$

which can be written in matrix form as follows,

$$\nabla\phi(\mathbf{r}; \mathbf{R}) + \boldsymbol{\tau}(\mathbf{R})\phi(\mathbf{r}; \mathbf{R}) = \mathbf{0} \quad (1.33)$$

Upon solving this first order differential equation in nuclear configuration space, we obtain

$$\phi(\mathbf{r}; \mathbf{R} : \mathbf{R}_0) = \mathcal{P}exp \left(- \int_{\mathbf{R}_0}^{\mathbf{R}} d\mathbf{R} \cdot \boldsymbol{\tau}(\mathbf{R}) \right) \phi(\mathbf{r}; \mathbf{R}_0) \quad (1.34)$$

where, the symbol \mathcal{P} signifies that the integration is being done in an order. For example, suppose the contour ($\mathbf{R}_0 \longrightarrow \mathbf{R}$) is divided in a grid of nuclear positions as, ($\mathbf{R}_0, \mathbf{R}_1, \mathbf{R}_2, \dots, \mathbf{R}$), then the integration is carried out for the limits ($\mathbf{R}_0, \mathbf{R}_1$), ($\mathbf{R}_1, \mathbf{R}_2$), ($\mathbf{R}_2, \mathbf{R}_3$),... in that order. The reason for using this approach is that $\boldsymbol{\tau}(\mathbf{R})$ in equation (1.34) is not a simple function, but a matrix. Also, \mathbf{R}_0 in $\phi(\mathbf{r}; \mathbf{R} : \mathbf{R}_0)$ in equation (1.34) suggests that the integration started from \mathbf{R}_0 .

If we compare equations (1.29) and (1.34), we obtain

$$\mathbf{A}(\mathbf{R}) = \mathcal{P}exp \left(- \int_{\mathbf{R}_0}^{\mathbf{R}} d\mathbf{R} \cdot \boldsymbol{\tau}(\mathbf{R}) \right) \quad (1.35)$$

We can also integrate the RHS of equation (1.34) over a closed contour in nuclear configuration space to get,

$$\phi(\mathbf{r}; \mathbf{R}_0 : \mathbf{R}_0) = \mathcal{P}exp \left(- \oint_{\Gamma} d\mathbf{R} \cdot \boldsymbol{\tau}(\mathbf{R}) \right) \phi(\mathbf{r}; \mathbf{R}_0) \quad (1.36)$$

where the symbol Γ represents a closed contour.

For a closed contour, the ADT matrix is replaced by the **Topological matrix** ($\mathbf{D}(\Gamma)$) and is given mathematically as,

$$\mathbf{D}(\Gamma) = \mathcal{P}exp \left(- \oint_{\Gamma} d\mathbf{R} \cdot \boldsymbol{\tau}(\mathbf{R}) \right) \quad (1.37)$$

The Topological matrix (like ADT matrix) is also an orthogonal matrix.

Since the electronic wavefunctions are self consistent, the wavefunction after being taken around the closed contour will be equal to the initial one up to a phase factor, that is

$$\phi_j(\mathbf{r}; \mathbf{R}_0 : \mathbf{R}_0) = exp(i\theta_j(\Gamma))\phi_j(\mathbf{r}; \mathbf{R}_0) \quad (1.38)$$

Because of this self consistency condition, the topological matrix is a diagonal matrix and its elements have the following form,

$$\mathbf{D}_{jk}(\Gamma) = \delta_{jk}exp(i\theta_j(\Gamma)) \quad (1.39)$$

where we have used the Kronecker delta, δ_{jk} so that off-diagonal terms of $\mathbf{D}(\Gamma)$ matrix become zero. Also, the electronic wavefunctions are assumed to be real, so θ_j will always be a multiple of π which means that the diagonal elements of the \mathbf{D} matrix can only be ± 1 . In summary, the electronic wavefunction after being taken around a closed contour in nuclear configuration space can be written as,

$$\phi_j(\mathbf{r}; \mathbf{R}_0 : \mathbf{R}_0) = \pm \phi_j(\mathbf{r}; \mathbf{R}_0) \quad (1.40)$$

provided the electronic wavefunctions are assumed to be real.

1.4 π Quantization Condition

We would like to use the concepts explained in section 1.3 to derive a quantitative condition to confirm the presence of a CI formed between two PESs. We will derive the condition for the simplest case, that is, considering only two electronic states. If we have only two states, then using equations (1.18) and (1.19), we can write the first-order NACT matrix as follows,

$$\boldsymbol{\tau}(\mathbf{R}) = \begin{pmatrix} 0 & \tau_{12}(\mathbf{R}) \\ -\tau_{12}(\mathbf{R}) & 0 \end{pmatrix}. \quad (1.41)$$

As we saw in the previous section, the ADT matrix is an orthogonal matrix, so it can be written as,

$$\mathbf{A}(\mathbf{R}) = \begin{pmatrix} \cos \gamma_{12}(\mathbf{R}) & \sin \gamma_{12}(\mathbf{R}) \\ -\sin \gamma_{12}(\mathbf{R}) & \cos \gamma_{12}(\mathbf{R}) \end{pmatrix} \quad (1.42)$$

where $\gamma_{12}(\mathbf{R})$ is called the **ADT angle**.

The NACT and ADT matrices obey the following first order differential equation,

$$\nabla \mathbf{A}(\mathbf{R}) + \boldsymbol{\tau}(\mathbf{R})\mathbf{A}(\mathbf{R}) = \mathbf{0} \quad (1.43)$$

which is just an extension of equation (1.33) which we derived in section 1.3. Substituting equations (1.41) and (1.42) in equation (1.43) and then simplifying, we obtain

$$\nabla \gamma_{12}(\mathbf{R}) + \tau_{12}(\mathbf{R}) = 0 \quad (1.44)$$

We can solve this first order differential equation for a contour in nuclear configuration space and obtain,

$$\gamma_{12}(\mathbf{R}) = \left(- \int_{\mathbf{R}_0}^{\mathbf{R}} d\mathbf{R} \cdot \tau_{12}(\mathbf{R}) \right). \quad (1.45)$$

Similarly, for a closed contour Γ in nuclear configuration space, we can write the Topological matrix (like ADT matrix) as,

$$\mathbf{D}(\Gamma) = \begin{pmatrix} \cos \alpha_{12}(\mathbf{R}) & \sin \alpha_{12}(\mathbf{R}) \\ -\sin \alpha_{12}(\mathbf{R}) & \cos \alpha_{12}(\mathbf{R}) \end{pmatrix}, \quad (1.46)$$

where $\alpha_{12}(\mathbf{R})$ is known as the **topological/geometrical phase**. We can write a similar equation for $\alpha_{12}(\mathbf{R})$, as we wrote for $\gamma_{12}(\mathbf{R})$ in equation (1.43), if we do an integration for closed contour Γ in nuclear configuration space,

$$\alpha_{12}(\mathbf{R}) = \left(- \oint_{\Gamma} d\mathbf{R} \cdot \tau_{12}(\mathbf{R}) \right) \quad (1.47)$$

We proved in section 1.3 (equation (1.39)) that the topological matrix is diagonal and if we examine the form of $\mathbf{D}(\Gamma)$ matrix from equation (1.46), it can be easily implied that the angle $\alpha_{12}(\mathbf{R})$ should be a multiple of π . So we can write equation (1.47) also as,

$$\alpha_{12}(\mathbf{R}) = \left(- \oint_{\Gamma} d\mathbf{R} \cdot \boldsymbol{\tau}_{12}(\mathbf{R}) \right) = n\pi \quad (1.48)$$

PESs of two electronic states $\phi_1(\mathbf{r}; \mathbf{R})$ and $\phi_2(\mathbf{r}; \mathbf{R})$ are forming a CI. Let's assume a closed loop Γ in nuclear configuration space. If $\phi_j(\mathbf{r}; \mathbf{R})(j = 1, 2)$ changes sign after being taken around the closed contour Γ , then there must be at least one nuclear configuration inside Γ at which $\phi_j(\mathbf{r}; \mathbf{R})(j = 1, 2)$ is discontinuous, which infers that the PES of $\phi_j(\mathbf{r}; \mathbf{R})(j = 1, 2)$ is forming a CI with that of another electronic state.⁷ This sign change of the electronic wavefunction is known as the *geometric phase effect*.⁸ According to this theorem, if we have a closed contour Γ enclosing a CI, then the concerned electronic wavefunctions can be written as,

$$\phi_j(\mathbf{r}; \mathbf{R}_0 : \mathbf{R}_0) = -\phi_j(\mathbf{r}; \mathbf{R}_0) \quad (1.49)$$

where \mathbf{R}_0 is any reference nuclear configuration on the closed loop Γ . In such a scenario, the Topological matrix $\mathbf{D}(\Gamma)$ can be written as follows,

$$\mathbf{D}(\Gamma) = \begin{pmatrix} -1 & 0 \\ 0 & -1 \end{pmatrix}, \quad (1.50)$$

If we compare equations (1.46) and (1.50), then it can be easily implied that the angle $\alpha_{12}(\mathbf{R})$ should be an odd multiple of π to obtain equation (1.50). Since we have only one CI inside the closed contour Γ , the *quantization condition* which confirms that two PESs are intersecting is given as,

$$\alpha_{12}(\mathbf{R}) = \left(- \oint_{\Gamma} d\mathbf{R} \cdot \boldsymbol{\tau}_{12}(\mathbf{R}) \right) = \pi \quad (1.51)$$

Similarly, if the loop surrounds two CIs, then $\alpha_{12}(\mathbf{R})$ should be equal to 2π ($n = 2$ in equation (1.48)), and the electronic wavefunction will not change sign after transporting it around the closed contour.

1.4.1 3-state Calculation

Many a time, considering only two states to achieve the quantization condition is not sufficient. Theoretically, if we choose a small loop encompassing a CI (implying that the

PESs of the concerned states are very close for that loop in nuclear coordinate space), then a two state calculation should be enough to reach the quantization condition, since at and around CI, non-adiabatic effects from other neighboring states are small. But in practical calculations, usually we work with closed contours which cover a large area in nuclear configuration space. In such cases, we have to include non-adiabatic interactions due to adjacent electronic states to attain the quantization condition. In this section, we will derive the requisite conditions incorporating three electronic states. To be more precise, we are assuming that PESs of states $\phi_1(\mathbf{r}; \mathbf{R})$ and $\phi_2(\mathbf{r}; \mathbf{R})$ are intersecting and we are including non-adiabatic effects due to $\phi_3(\mathbf{r}; \mathbf{R})$ to help us achieve π quantization.

The NACT matrix for a 3-state case can be written as,

$$\boldsymbol{\tau}(\mathbf{R}) = \begin{pmatrix} 0 & \tau_{12}(\mathbf{R}) & \tau_{13}(\mathbf{R}) \\ -\tau_{12}(\mathbf{R}) & 0 & \tau_{23}(\mathbf{R}) \\ -\tau_{13}(\mathbf{R}) & -\tau_{23}(\mathbf{R}) & 0 \end{pmatrix}. \quad (1.52)$$

Since the ADT matrix is an orthogonal matrix, it can be written as a product of three orthogonal matrices in the following way,

$$\mathbf{A}(\mathbf{R}) = \mathbf{Q}_{12}(\mathbf{R})\mathbf{Q}_{23}(\mathbf{R})\mathbf{Q}_{13}(\mathbf{R}) \quad (1.53)$$

where

$$\mathbf{Q}_{12}(\mathbf{R}) = \begin{pmatrix} \cos \gamma_{12}(\mathbf{R}) & \sin \gamma_{12}(\mathbf{R}) & 0 \\ -\sin \gamma_{12}(\mathbf{R}) & \cos \gamma_{12}(\mathbf{R}) & 0 \\ 0 & 0 & 1 \end{pmatrix} \quad (1.54a)$$

$$\mathbf{Q}_{23}(\mathbf{R}) = \begin{pmatrix} 1 & 0 & 0 \\ 0 & \cos \gamma_{23}(\mathbf{R}) & \sin \gamma_{23}(\mathbf{R}) \\ 0 & -\sin \gamma_{23}(\mathbf{R}) & \cos \gamma_{23}(\mathbf{R}) \end{pmatrix} \quad (1.54b)$$

$$\mathbf{Q}_{13}(\mathbf{R}) = \begin{pmatrix} \cos \gamma_{13}(\mathbf{R}) & 0 & \sin \gamma_{13}(\mathbf{R}) \\ 0 & 1 & 0 \\ -\sin \gamma_{13}(\mathbf{R}) & 0 & \cos \gamma_{13}(\mathbf{R}) \end{pmatrix} \quad (1.54c)$$

where $\gamma_{12}(\mathbf{R})$, $\gamma_{23}(\mathbf{R})$, and $\gamma_{13}(\mathbf{R})$ are the corresponding ADT angles for the coupling between the three electronic states.

If we substitute equations (1.52) and (1.53) in equation (1.43) and simplify, then we

obtain the following system of coupled differential equations.

$$\begin{aligned}
 \nabla \gamma_{12}(\mathbf{R}) &= -\tau_{12}(\mathbf{R}) - \tan \gamma_{23}(\mathbf{R})(-\tau_{13}(\mathbf{R}) \cos \gamma_{12}(\mathbf{R}) + \tau_{23}(\mathbf{R}) \sin \gamma_{12}(\mathbf{R})) \\
 \nabla \gamma_{23}(\mathbf{R}) &= -(\tau_{23}(\mathbf{R}) \cos \gamma_{12}(\mathbf{R}) + \tau_{13}(\mathbf{R}) \sin \gamma_{12}(\mathbf{R})) \\
 \nabla \gamma_{13}(\mathbf{R}) &= (\cos \gamma_{13}(\mathbf{R}))^{-1}(-\tau_{13}(\mathbf{R}) \cos \gamma_{12}(\mathbf{R}) + \tau_{23}(\mathbf{R}) \sin \gamma_{12}(\mathbf{R}))
 \end{aligned}
 \tag{1.55}$$

Since PESs of $\phi_1(\mathbf{r}; \mathbf{R})$ and $\phi_2(\mathbf{r}; \mathbf{R})$ are forming a CI, we will solve equation (1.55) for $\gamma_{12}(\mathbf{R})$ for a closed contour enclosing the concerned CI in the nuclear coordinate space.

1.5 Potential Energy Surfaces (PESs)

Let us consider equation (1.5) which is the electronic time-independent Schrödinger equation. Since the electronic wavefunction described in section 1.2.1 depends parametrically on the nuclear coordinates, if we change the nuclear configuration slightly from \mathbf{R}'' to \mathbf{R}' , then the electronic wavefunction will adjust from $\phi_j(\mathbf{r}; \mathbf{R}'')$ to $\phi_j(\mathbf{r}; \mathbf{R}')$ (electrons respond instantly to this nuclear change). Consequently, the electronic energy will also change from $E_j(\mathbf{R}'')$ to $E_j(\mathbf{R}')$, therefore we can say that as the nuclear configuration of the molecule changes, the electronic energy varies smoothly as a function of the nuclear coordinates. Thus, $E_j(\mathbf{R})$ can also be considered as the *potential energy* for the nuclear motion for the j th electronic state.⁹ Since there are innumerable nuclear configurations, we can solve equation (1.5) for each of these configurations and get the corresponding energy $E_j(\mathbf{R})$ and form the PES for the nuclear motion.

1.6 Non-adiabatic Processes and Conical Intersections (CIs)

The nuclear motion is confined to a single PES within the framework of Born-Oppenheimer approximation. But there are processes known in chemistry where the nuclear motion is no longer restricted to one PES and they are called *Non-adiabatic processes*. Some of the important chemical processes governed by non-adiabatic theory are vision, charge transfer reactions, light harvesting, and numerous reactions happening in the upper atmosphere. In such processes, there is a strong coupling between nuclear and electronic motion due to which the nuclear and electronic wavefunctions cannot be considered as separate entities and we say that there is a breakdown of Born-Oppenheimer approximation. Of course, these processes are mostly prevalent in regions of nuclear configuration

space where the PESs are in close proximity. The places where the PESs intersect are called *Conical Intersections (CIs)* and they are at the heart of most of the non-adiabatic phenomena. CIs can induce ultrafast decay of excited electronic states due to the large interstate coupling near the crossing. They can also facilitate lower state to upper state (LtU) transitions.⁸ CIs can lead to the formation of more than one product if the reaction is directed through them instead of a transition state.

Let us consider a CI formed by two PESs. Now, for the two PESs to cross, the electronic Hamiltonian matrix at CI must satisfy certain conditions. The Hamiltonian matrix is given as follows,¹⁰

$$\mathbf{H} = \begin{pmatrix} H_{11} & H_{12} \\ -H_{12} & H_{22} \end{pmatrix} \quad (1.56)$$

At CI,

$$H_{11} = H_{22} \quad (1.57)$$

and

$$H_{12} = 0 \quad (1.58)$$

A *seam* can be defined as the locus formed by the points of CI when two PESs intersect. The dimension of seam of CI is of particular importance for a proper understanding of CIs and non-adiabatic processes.

Now, CIs can be broadly classified into three types¹¹

Symmetry-required intersections

The symmetry of the electronic states forming CI are components of multi-dimensional irreducible representation of a point group (for example, the irreducible representation E in C_{4v} point group). In such cases, both the conditions (equations (1.57) and (1.58)) are satisfied using symmetry arguments. So, the molecule must have sufficient symmetry to have these type of CIs. The seam dimension is $N_{int.}$ ($N_{int.}$ is the number of internal degrees of freedom available to the molecule) since no degree of freedom is being used to satisfy the two *conditions*.

Accidental symmetry-allowed intersections

The symmetry of the states forming the CI have different one-dimensional irreducible representation. Here, $H_{12} = 0$ by symmetry but since the intersection is accidental, so $H_{11} = H_{22}$ by chance. The dimension of seam is $(N_{int.} - 1)$, since one degree of freedom got consumed in order to satisfy equation (1.57).

Accidental same-symmetry intersections

The symmetry of the states forming the CI have the same one-dimensional irreducible representation. Both the conditions are being satisfied by accident. The dimension of the seam of CI in this case is $(N_{int.} - 2)$, since two degrees of freedom are required to fulfill the two conditions.

CIs can also be distinguished based on the nature of dependence of potential energy on nuclear coordinates in the vicinity of CI (figure 1.1).

Renner-Teller CI (RT CI)

The potential energy depends quadratically on nuclear coordinates near CI (the linear energy term in the Schrödinger equation given by equation (1.27) goes to zero in such cases). RT CIs are usually associated with linear molecules.¹² They are also called glancing CIs.

Jahn-Teller CI (JT CI)

The potential energy varies linearly as a function of nuclear parameters in the neighborhood of CI. The local topology near the crossing is like a double cone, so it is simply known as a *conical intersection*.

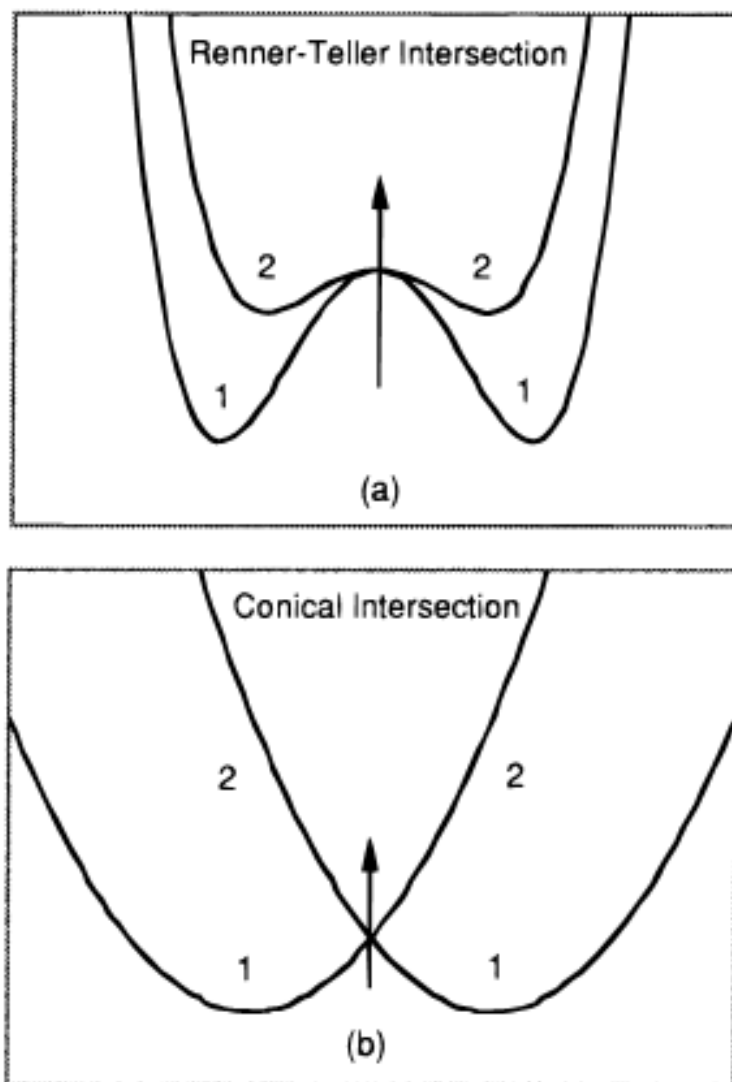


Figure 1.1: Section of (a) Renner-Teller CI and (b) a general or Jahn-Teller CI.¹³

Chapter 2

Results & Discussion

2.1 Computational Details

The molecule of our interest is linear HeH_2^+ . It has only 3 electrons. The atoms forming the molecule are Hydrogen (H) and Helium (He). Both H and He have $1s$ as the only occupied orbital in the ground state.

Our aim is to study the PES diagram for HeH_2^+ molecule and then see if we have any potential CIs formed by PESs. If the PES diagram is showing a CI between two states, then we will be using Non-adiabatic coupling theory explained in chapter 1 to confirm the presence of the CI. As we described in section 1.4, we have to calculate NACTs and ADT angles for the concerned electronic states forming the CI and also for additional adjacent electronic states to achieve the π quantization condition. We did all the calculations using the MOLPRO package¹⁴. As is evident from equation (1.11), NACTs are calculated using the electronic wavefunctions, so the wavefunctions were calculated using CASSCF (complete active space self consistent field) and MRCI (multi-reference configuration interaction) theory, and aug-cc-pVTZ basis set. The symmetry of the molecule was chosen to be C_s and the lowest 3 a' orbitals were included in the *active space* for the calculation of electronic wavefunctions. We considered only the doublet states, more specifically, the lowest three $^2A'$ states in all the calculations.

HeH_2^+ is a tri-atomic molecule which means that all the atoms will lie on a single plane in any geometrical configuration. To do the necessary calculations, we need to form a closed contour (enclosing a CI) in nuclear configuration space and the simplest way to do that on a single plane is to choose a circular contour as shown in Figure 2.1, where the atom \mathbf{X} is just a dummy atom and is used to help us to make closed contours.

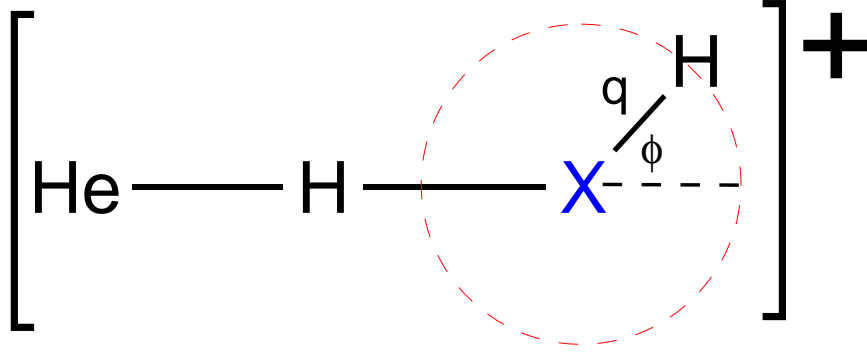


Figure 2.1: HeH_2^+ molecule with a closed contour (in red) in nuclear configuration space

The dummy atom also allows us to cover any desired area in the nuclear configuration space. \mathbf{X} does not interfere with the calculations.

If we trace a circular contour as shown in Figure 2.1, then the only nuclear coordinate that is changing is ϕ provided all the bond distances and the radius of the contour (q) are kept constant. So we can rewrite some of the important equations stated in chapter 1 as,

$$\tau_{ij}(\phi) = \langle \phi_i | \nabla \phi_j \rangle \quad (2.1)$$

$$\gamma_{12}(\phi) = \left(- \int_0^{2\pi} \tau_{12}(\phi) d\phi \right). \quad (2.2)$$

$$\begin{aligned} \nabla \gamma_{12}(\phi) &= -\tau_{12}(\phi) - \tan \gamma_{23}(\phi) (-\tau_{13}(\phi) \cos \gamma_{12}(\phi) + \tau_{23}(\phi) \sin \gamma_{12}(\phi)) \\ \nabla \gamma_{23}(\phi) &= -(\tau_{23}(\phi) \cos \gamma_{12}(\phi) + \tau_{13}(\phi) \sin \gamma_{12}(\phi)) \\ \nabla \gamma_{13}(\phi) &= (\cos \gamma_{13}(\phi))^{-1} (-\tau_{13}(\phi) \cos \gamma_{12}(\phi) + \tau_{23}(\phi) \sin \gamma_{12}(\phi)) \end{aligned} \quad (2.3)$$

We calculated NACTs ($\tau_{12}, \tau_{23}, \tau_{13}$) using the MOLPRO package.¹⁴ After obtaining the NACTs the 2-state ADT angle (equation (2.2)) was calculated using a numerical integration method called the *Trapezoidal rule*. We made a code using Fortran programming language for the trapezoidal rule to calculate the ADT angle. The ADT angle for the 3-state case was calculated by solving the coupled differential equations given by equation (2.3). We used *ode45* (Runge-Kutta (4,5) method) method in MATLAB to solve this system of coupled differential equations. The data for NACT, ADT angle and energy were plotted using MATLAB.

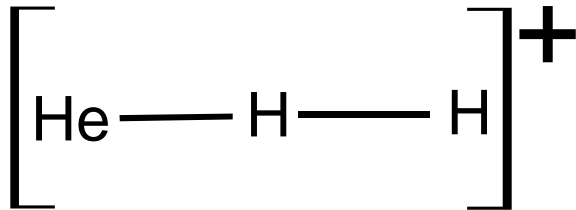


Figure 2.2: Linear HeH_2^+ molecule

2.2 Linear HeH_2^+

The nuclear configuration of linear HeH_2^+ molecule is shown in Figure 2.2. We plotted the 3-D PES diagram for the lowest three doublet states for linear HeH_2^+ (Figure 2.3). For the 3-D plot, the x-axis, y-axis, and z-axis were chosen to be the He-H bond length (\AA), H-H bond length (\AA), and the potential energy (Hartree) of the molecule as a function of these bond distances, respectively. Since in the linear geometry, the point group of HeH_2^+ is $D_{\infty h}$, the states are designated as $^2\Sigma^+$. As can be seen from Figure 2.3, there is considerable energy difference between the ground state ($1^2\Sigma^+$) and the first excited state ($2^2\Sigma^+$). But the first and the second excited states are coming close to each other in a particular region of nuclear configuration space. We have enlarged and re-orientated this region so that we can clearly see how these two PESs are approaching each other. From Figure 2.4, it can be seen that the first two excited states are probably forming a point of degeneracy at a specific molecular geometry. From the data, the molecular geometry at which the PESs are closest to each other was found to be $R(\text{He-H})= 0.8\text{\AA}$ and $R(\text{H-H})= 0.7\text{\AA}$.

Now that we know the molecular geometry at which PESs are forming a CI, we can go on to make a closed contour enclosing this CI and then calculate NACT and ADT angle for this closed contour to get the required π quantization and confirm the presence of the CI. We can form the closed contour in the following two ways as shown in Figure 2.5. As we can see from Figure 2.5, both the schemes show the same molecule but with some differences. In Scheme-1, the He-H and H-X bond distances are 0.8\AA and 0.8\AA , respectively and the H atom is being rotated about X to form the closed contour. Whereas, in Scheme-2, the H-H and H-X bond distances are 0.7\AA and 0.8\AA , respectively and the He atom is being rotated about X to make the closed contour.

Since we are doing calculations for the confirmation of CI formed by 2nd and 3rd state ((2,3) CI), so we have to calculate γ_{23} as a function of ϕ . The quantization condition

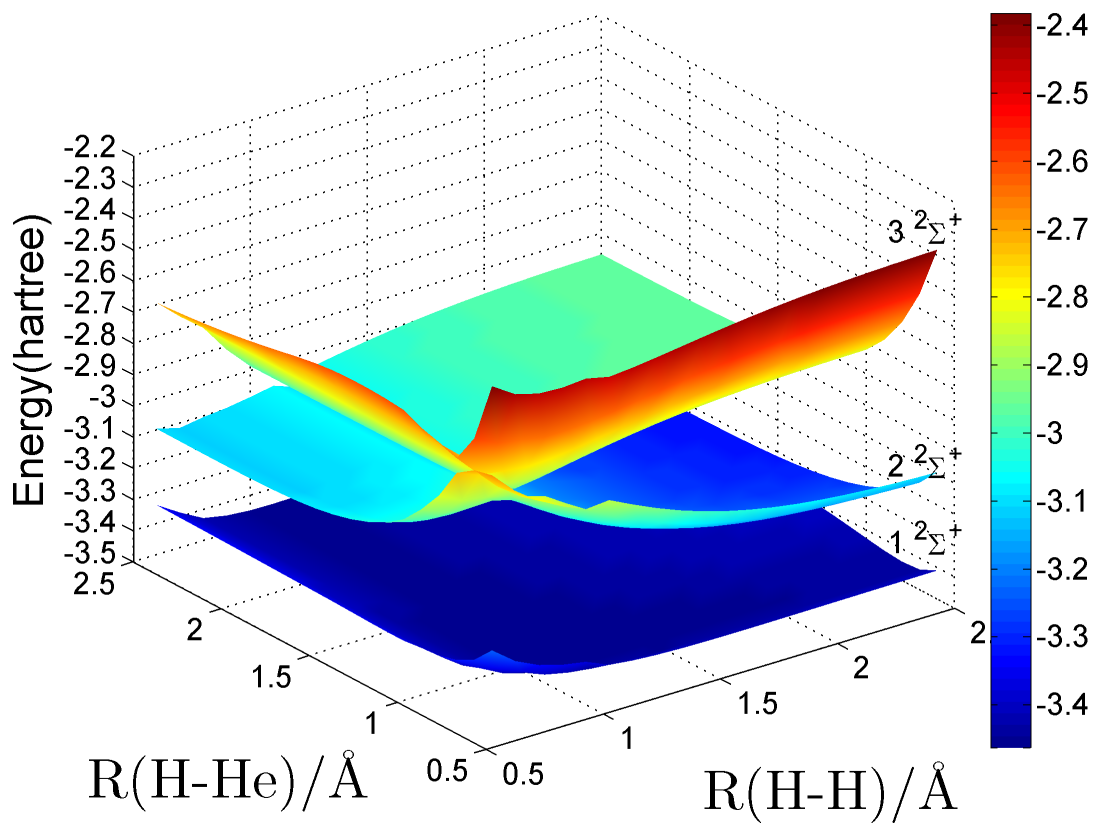


Figure 2.3: PES diagram depicting the lowest three states for linear HeH₂⁺

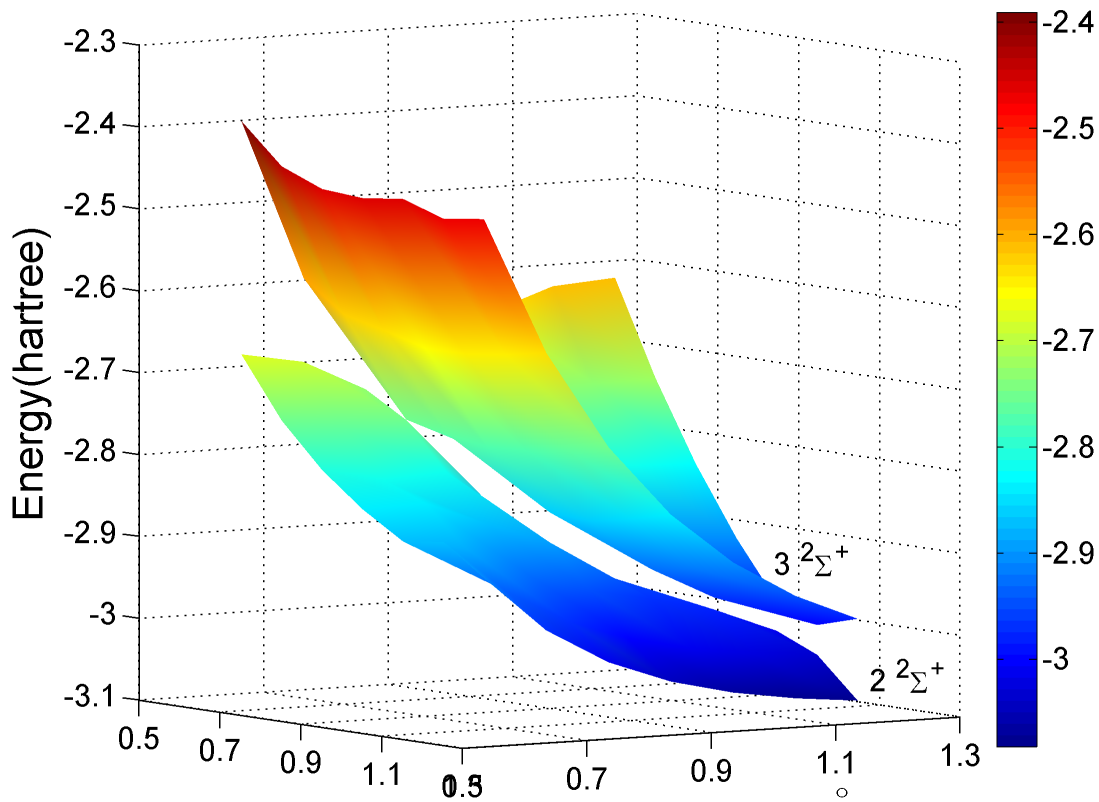


Figure 2.4: Close-up view of the region where the PESs of the two lowest excited states are close to each other (for linear HeH_2^+)

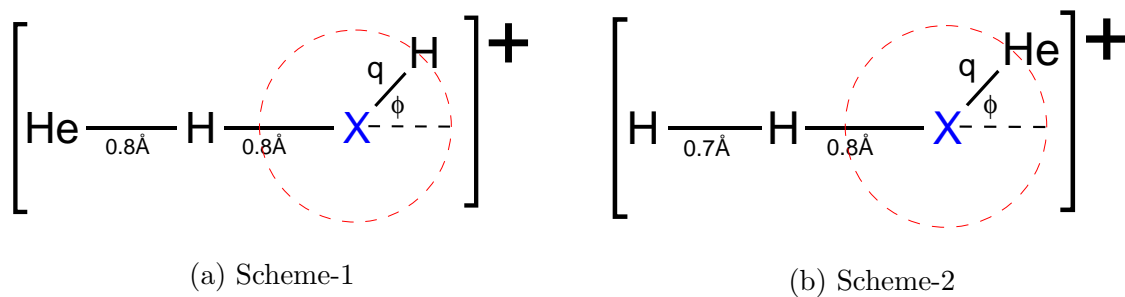


Figure 2.5: Molecular configuration of HeH_2^+ used to calculate NACTs and ADT angle

which we would like to achieve is,

$$\gamma_{23}(\phi = 2\pi) = \alpha_{23} = \pi \quad (2.4)$$

where α_{23} is the corresponding geometrical phase. We have to calculate $\gamma_{23}(\phi)$ using both 2- and 3-state methods. The equation for 2-state is same as equation (2.2),

$$\gamma_{23}(\phi) = \left(- \int_0^{2\pi} \tau_{23}(\phi) d\phi \right). \quad (2.5)$$

but we have to change the 3-state equation given by equation (2.3). We derived the 3-state equation in section 1.4.1 taking the three coupling terms in the order (12) \times (23) \times (13) where we solved for (1,2) CI. But since we are looking for (2,3) CI, we have to derive the 3-state equation by considering the order of coupling terms as (23) \times (13) \times (12). Doing this will give us a slightly different form of equation (2.3) which is,¹⁵

$$\begin{aligned} \nabla \gamma_{23}(\phi) &= -\tau_{23}(\phi) - \tan \gamma_{13}(\phi)(-\tau_{13}(\phi) \cos \gamma_{23}(\phi) + \tau_{12}(\phi) \sin \gamma_{23}(\phi)) \\ \nabla \gamma_{13}(\phi) &= -(\tau_{12}(\phi) \cos \gamma_{23}(\phi) + \tau_{13}(\phi) \sin \gamma_{23}(\phi)) \\ \nabla \gamma_{12}(\phi) &= (\cos \gamma_{13}(\phi))^{-1}(-\tau_{12}(\phi) \cos \gamma_{23}(\phi) + \tau_{13}(\phi) \sin \gamma_{23}(\phi)) \end{aligned} \quad (2.6)$$

2.2.1 Scheme-1

We calculated NACTs (τ_{12} , τ_{23} , τ_{13}), 2-state and 3-state ADT angle (γ_{23}), and energy for different q values and then plotted them with respect to ϕ for the molecular configuration designated as Scheme-1. We did calculations for $q = 0.1, 0.2, 0.3, 0.4, 0.6, 1.0, 1.3, 1.5, 1.8 \text{ \AA}$.

From the PES diagram, we found the nuclear configuration at which there is a CI (formed by the lowest two excited states) and that is $R(\text{He-H}) = 0.8 \text{ \AA}$ and $R(\text{H-H}) = 0.7 \text{ \AA}$. The molecule represented by Scheme-1 attains this geometry for $q = 0.1 \text{ \AA}$ and $\phi = \pi$. Due to this, τ_{23} shows a sharp peak (Figure 2.6a) and the $2^2A'$ and $3^2A'$ PECs form the concerned CI (Figure 2.6d) at $\phi = \pi$.

For $q = 0.1 \text{ to } 0.6 \text{ \AA}$ (Figures 2.6, 2.7, 2.8, 2.9, 2.10), from the plots of NACTs it is clear that the magnitude of τ_{23} is the largest which is expected since we are near to (2,3) CI and hence the $2^2A'$ and $3^2A'$ states are also close. The magnitude of other NACTs, τ_{12} and τ_{13} , is very less as compared to τ_{23} since there is considerable energy difference between $1^2A'$ and $2^2A'$. The plots of ADT angle show us the value of $\gamma_{23}(\phi = 2\pi)$. For $q = 0.1, 0.2 \text{ \AA}$, $\gamma_{23}(\phi = 2\pi)$ is close to (but slightly less than) π . It's almost exactly equal

to π for $q = 0.3, 0.4\text{\AA}$, and for $q = 0.6\text{\AA}$, it is a tad greater than π . Also, there is not much difference between the 2-state and 3-state results for the ADT angle. Thus, we can say that π quantization is achieved in all cases but still there is room for improvement for some q values.

For $q = 1.0, 1.3, 1.5\text{\AA}$ (Figures 2.11, 2.12, 2.13), the H atom which is forming the closed contour, is coming very near to He and the other H atom for ϕ close to π . In this case, the magnitude of all three NACTs ($\tau_{12}, \tau_{23}, \tau_{13}$) are very small and they are almost equivalent to each other. For this reason, we didn't plot the ADT angle for these q values because it was clear from the data (both 2- and 3-state) that the $\gamma_{23}(\phi = 2\pi)$ won't even reach $\pi/2$ let alone π . Although we are sure that the loop is enclosing the CI, but since the radius of the contour is large which means we are moving far from the CI and hence the coupling terms are small. Maybe we will have to redo the calculations taking other adjacent electronic states into account.

Now, $q = 1.8\text{\AA}$ (Figure 2.14) is an exceptional case for Scheme-1. The reason for this anomaly is probably due to the molecular structure change from $[\text{He-H-H}]^+$ to $[\text{H-He-H}]^+$ as the H atom moves around the circular contour. The PEC diagram (Figure 2.14c) shows that $1^2A'$ and $2^2A'$ are quite close to each other due to which τ_{12} has a very large magnitude with two sharp peaks. Therefore, we calculated γ_{12} instead of γ_{23} and coincidentally $\gamma_{12}(\phi = 2\pi)$ is reasonably close to π (Figure 2.14b). Based on this observation, we can say that the path of the circle is fairly close to a (1,2) CI but not necessarily for a linear geometry. If we vary the bond angle along with bond distances, then there can be infinitely many other candidate nuclear configurations for a CI (more on this in section 2.3).

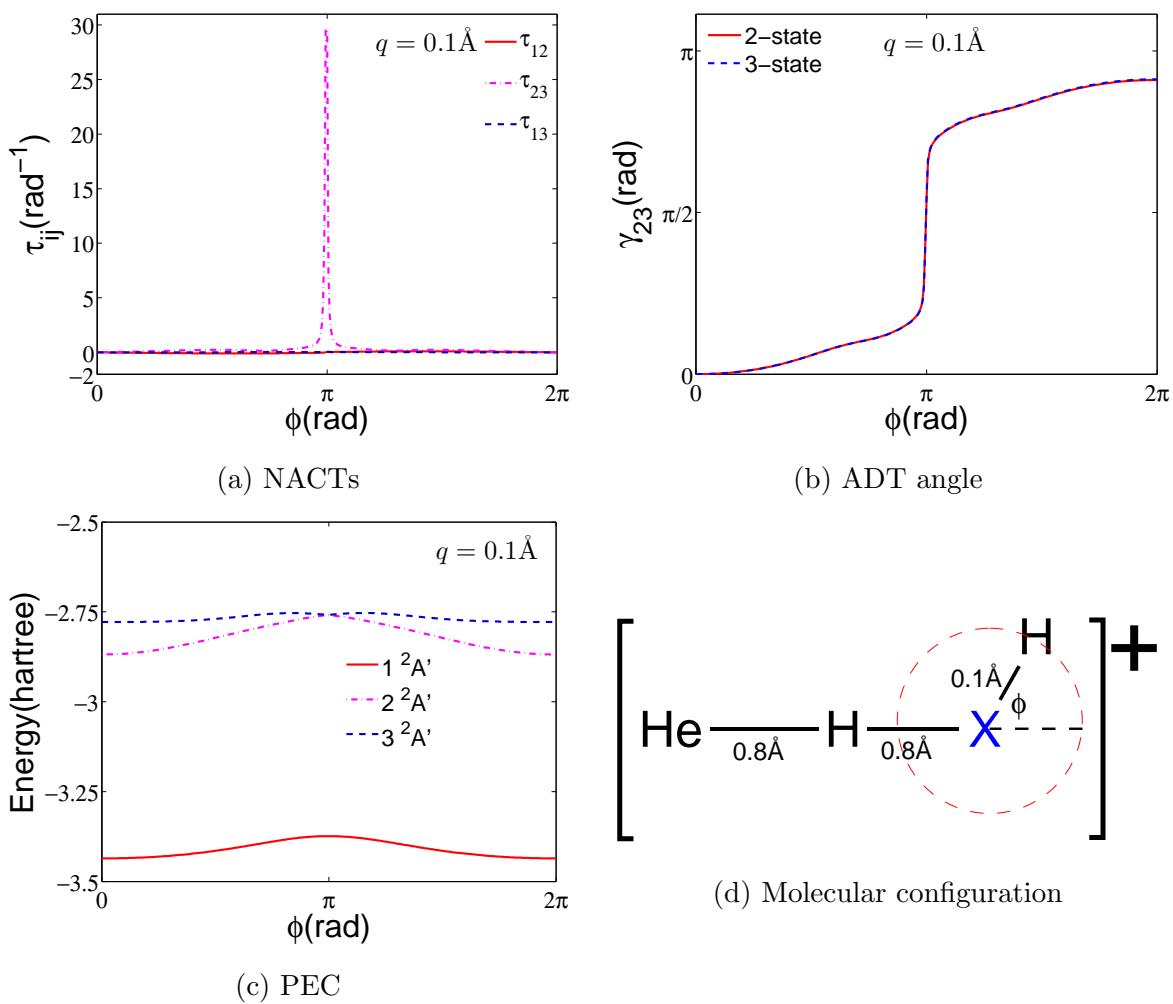


Figure 2.6: Plots of NACTs, ADT angle, and energy as a function of ϕ for $q = 0.1\text{\AA}$ of Scheme-1

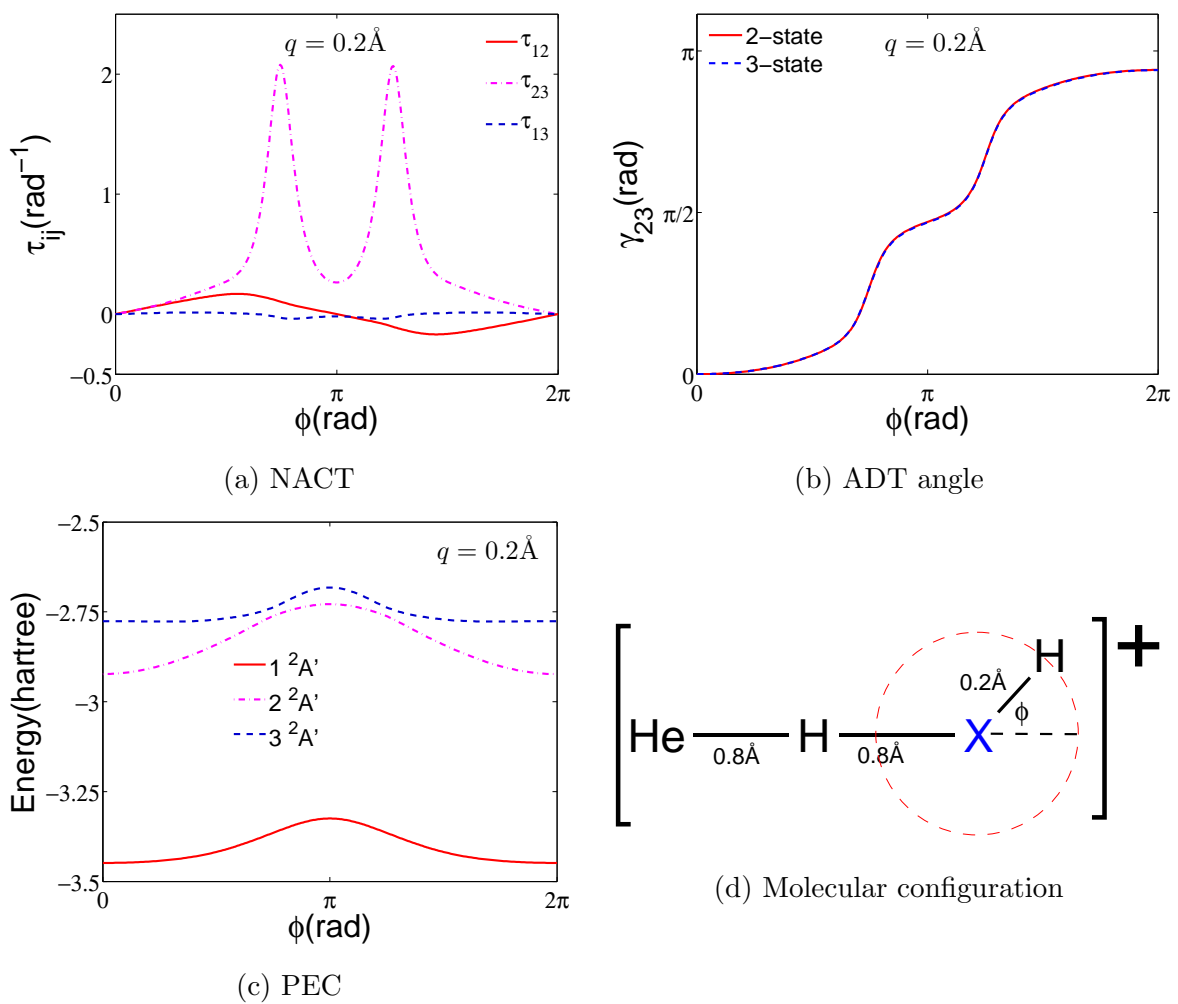


Figure 2.7: Plots of NACTs, ADT angle, and energy as a function of ϕ for $q = 0.2\text{\AA}$ of Scheme-1

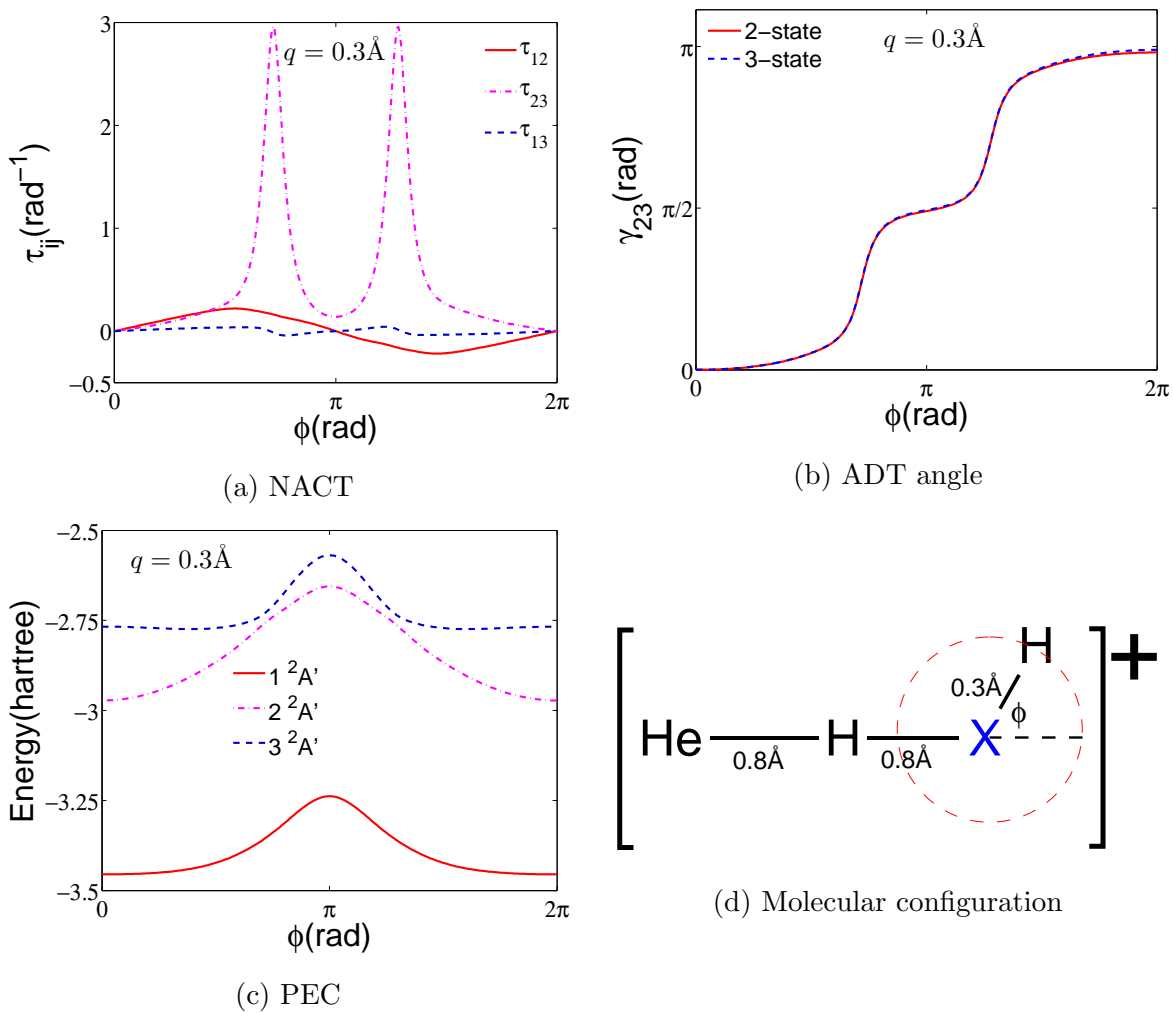


Figure 2.8: Plots of NACTs, ADT angle, and energy as a function of ϕ for $q = 0.3\text{\AA}$ of Scheme-1

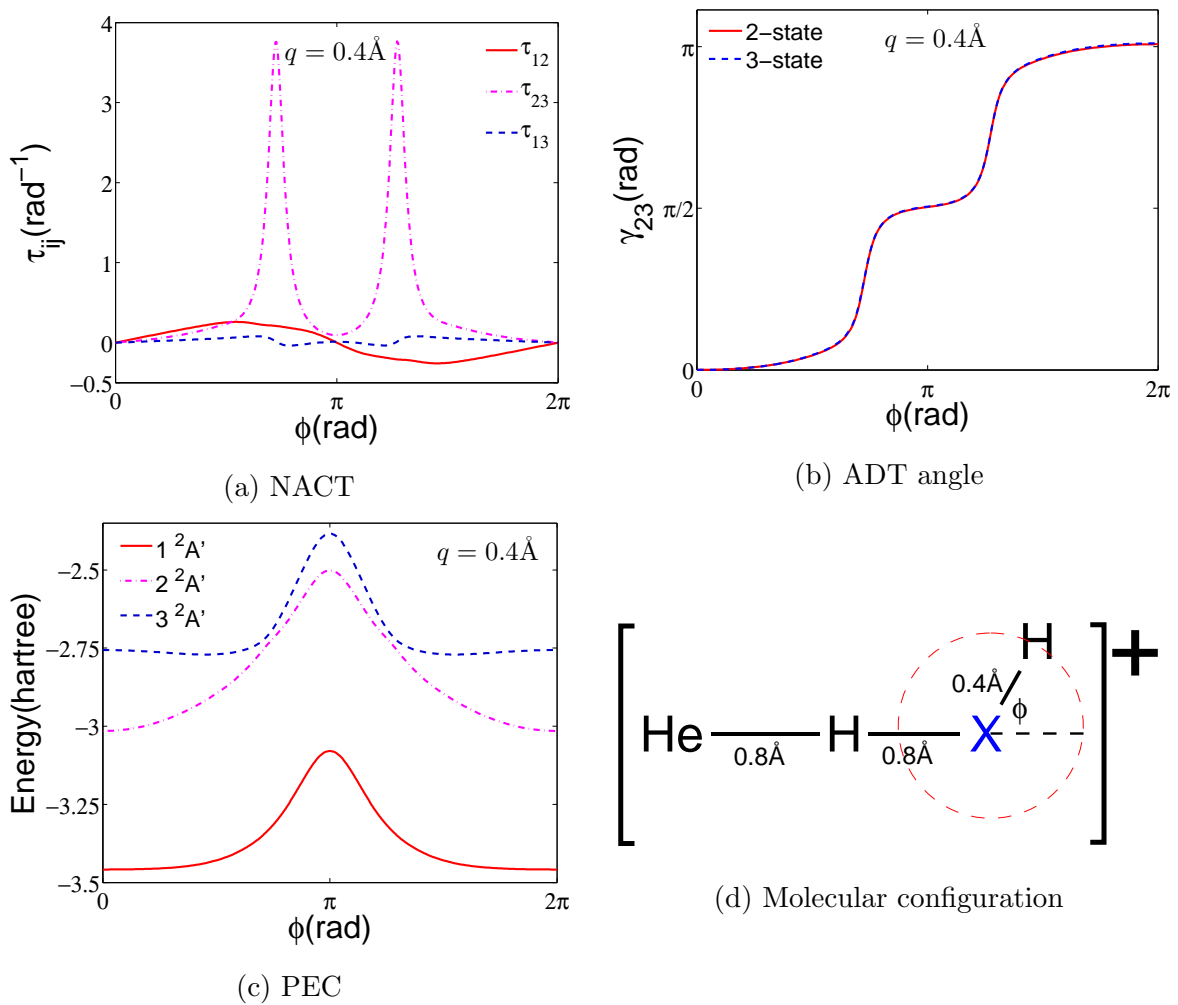


Figure 2.9: Plots of NACTs, ADT angle, and energy as a function of ϕ for $q = 0.4\text{\AA}$ of Scheme-1

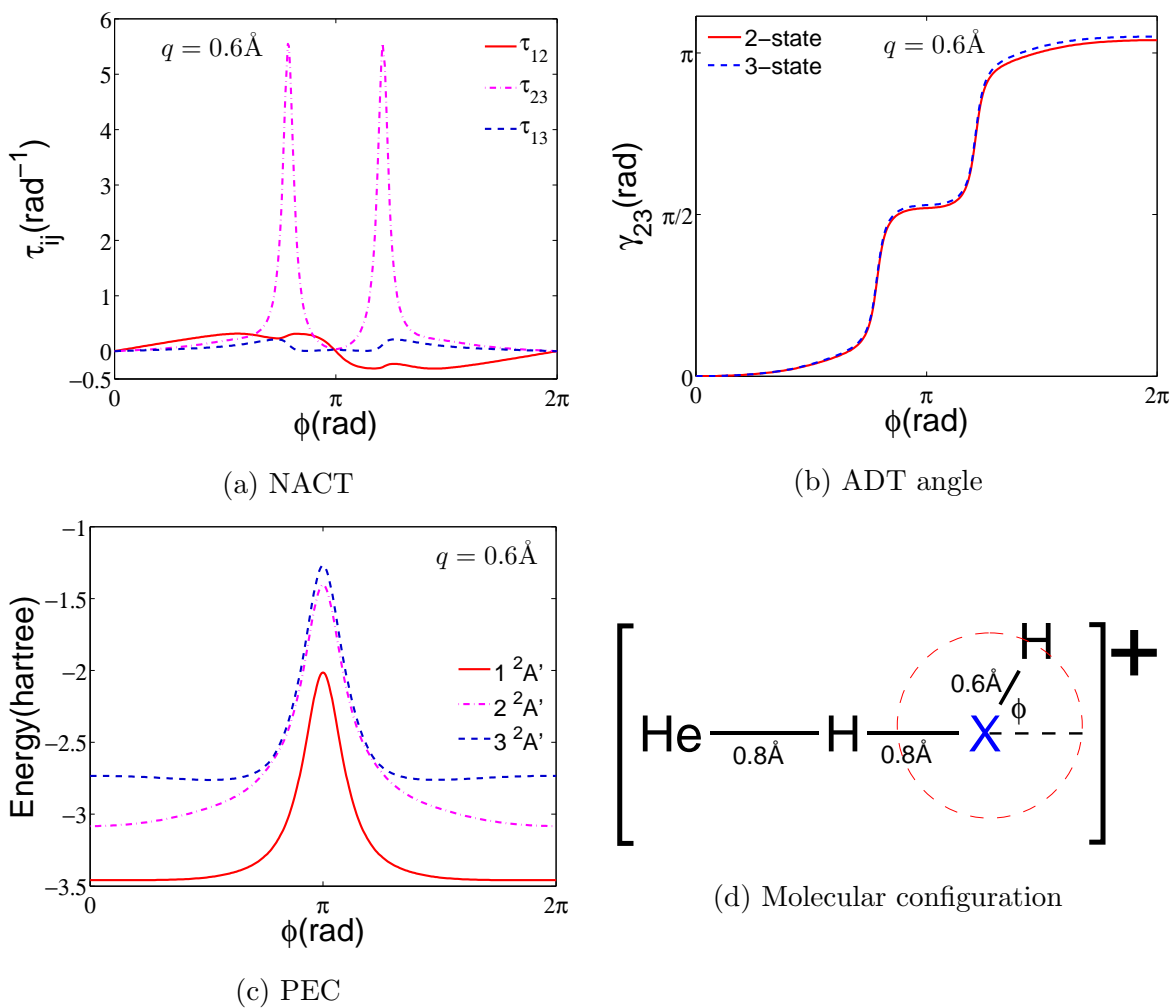


Figure 2.10: Plots of NACTs, ADT angle, and energy as a function of ϕ for $q = 0.6\text{\AA}$ of Scheme-1

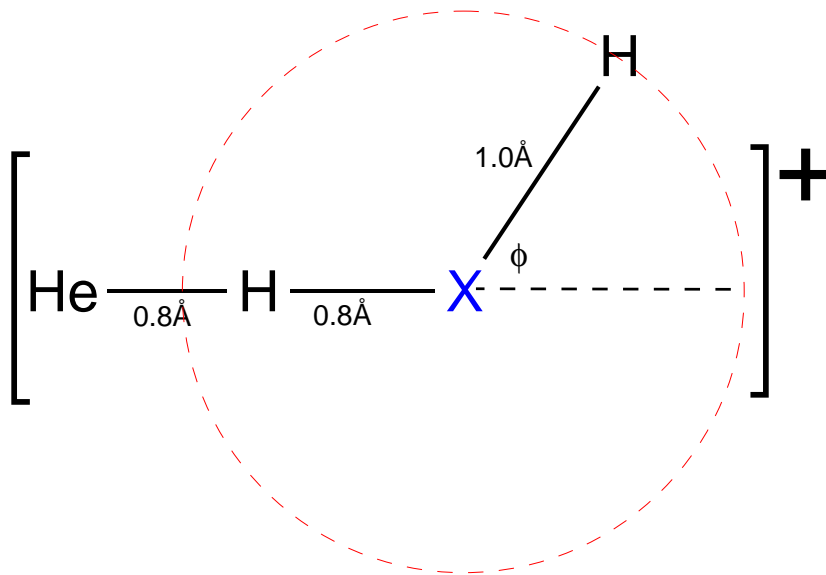
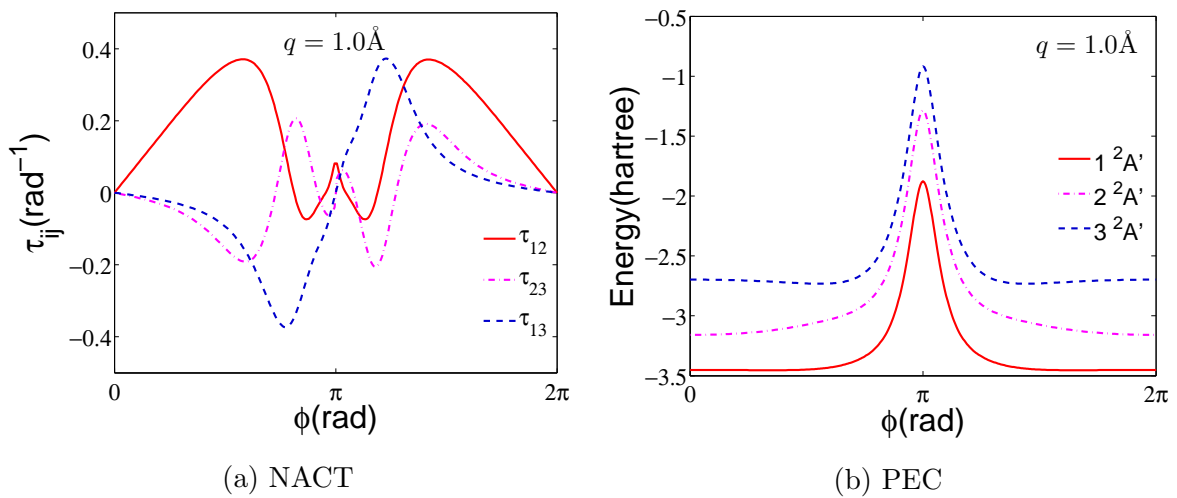
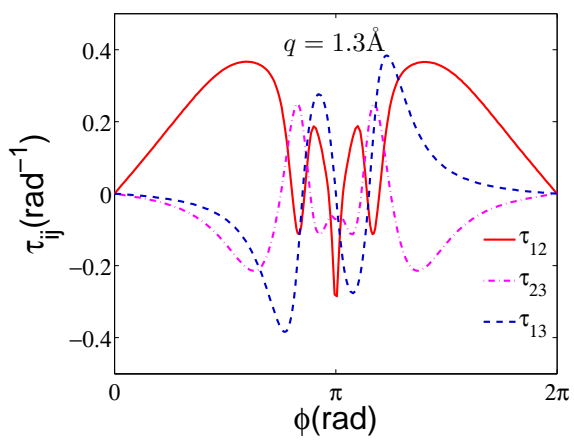
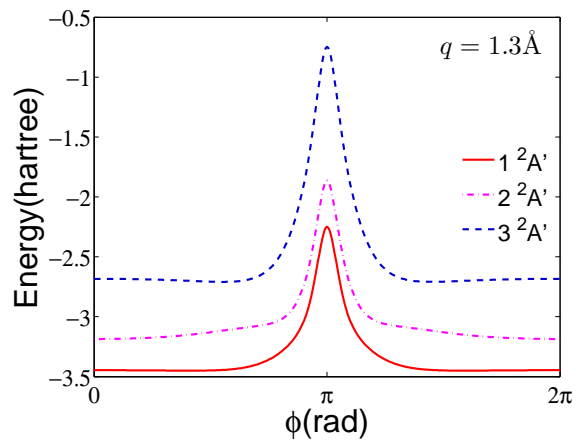


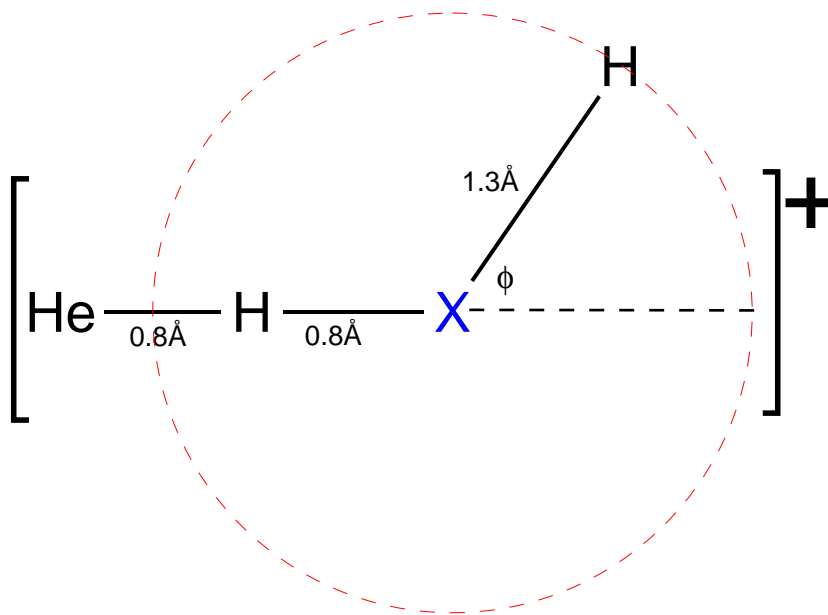
Figure 2.11: Plots of NACTs, and energy as a function of ϕ for $q = 1.0 \text{ \AA}$ of Scheme-1



(a) NACT

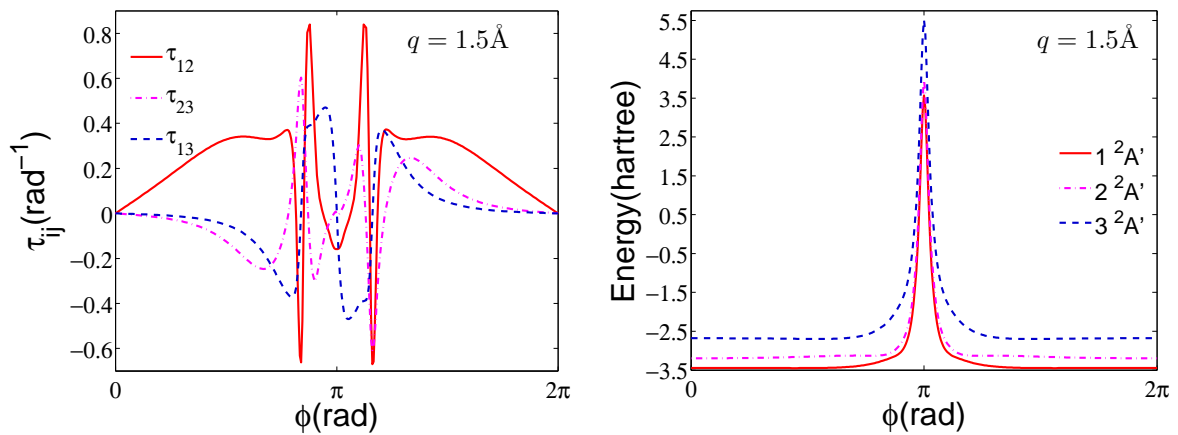


(b) PEC



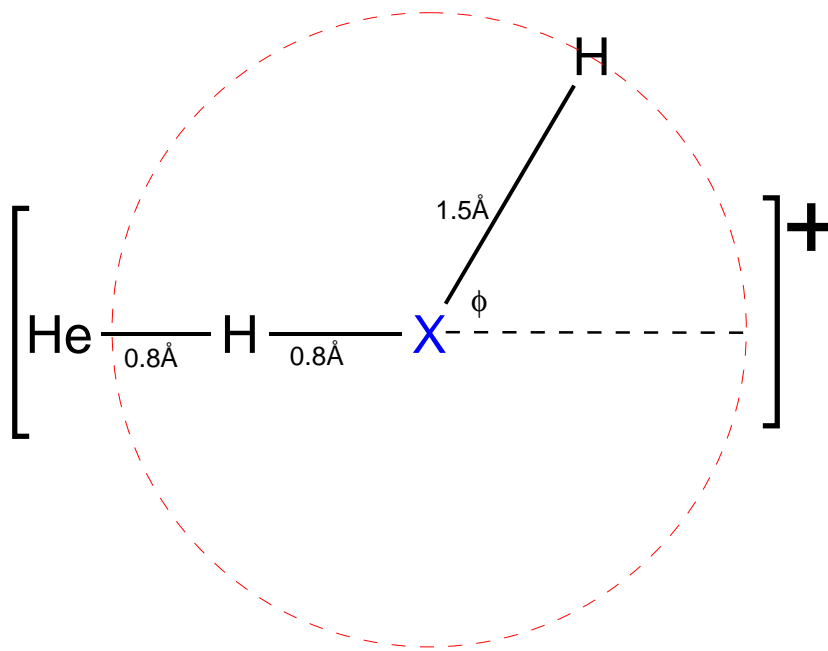
(c) Molecular configuration

Figure 2.12: Plots of NACTs, and energy as a function of ϕ for $q = 1.3\text{\AA}$ of Scheme-1



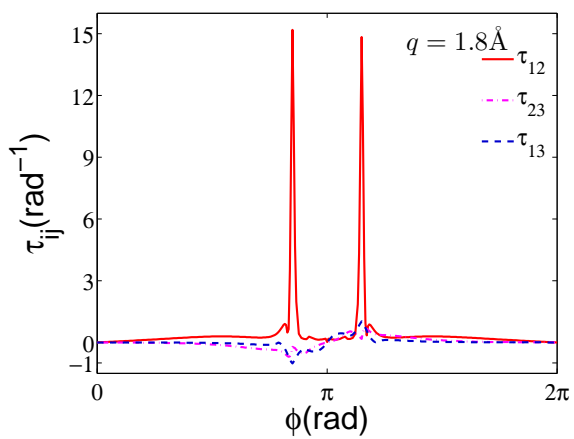
(a) NACT

(b) PEC

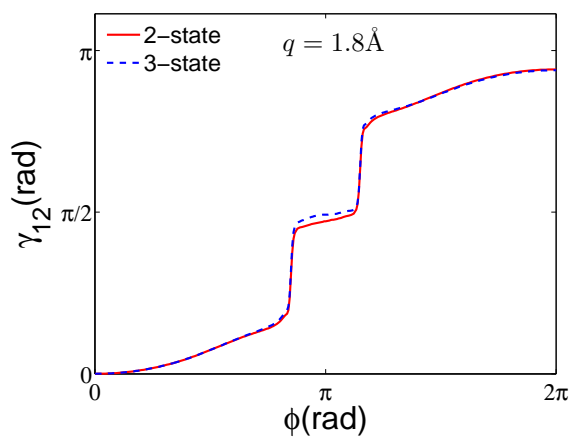


(c) Molecular configuration

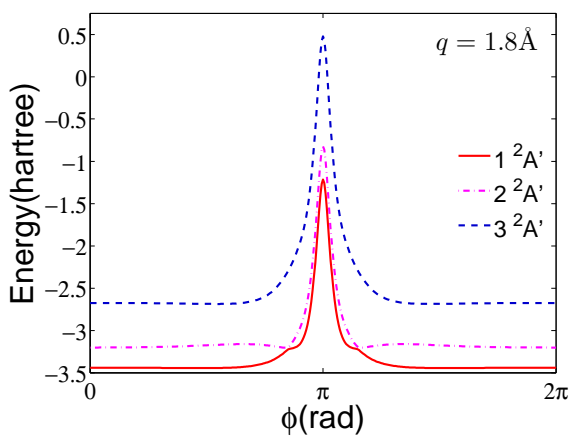
Figure 2.13: Plots of NACTs, and energy as a function of ϕ for $q = 1.5\text{\AA}$ of Scheme-1



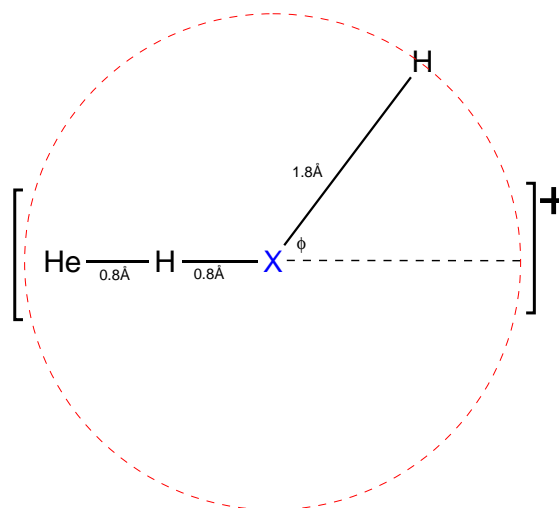
(a) NACT



(b) ADT angle



(c) PEC



(d) Molecular configuration

Figure 2.14: Special case: Plots of NACTs, ADT angle, and energy as a function of ϕ for $q = 1.8\text{\AA}$ of Scheme-1

2.2.2 Scheme-2

Similarly, for Scheme-2, NACTs ($\tau_{12}, \tau_{23}, \tau_{13}$), 2-state and 3-state ADT angle (γ_{23}), and energy were calculated for different q values and then plotted with respect to ϕ . For Scheme-2, we took $q = 0.1, 0.2, 0.3, 0.4, 0.6, 1.0, 1.2, 1.8 \text{ \AA}$.

When $q = 0.1 \text{ to } 0.6 \text{ \AA}$ (Figures 2.15, 2.16, 2.17, 2.18, 2.19), the path of closed contour is close to (2,3) CI and we can see from PEC diagrams that $2^2A'$ and $3^2A'$ are in proximity compared to $1^2A'$ due to which the magnitude of τ_{23} is relatively larger than the other two NACTs (τ_{12}, τ_{13}). Regarding the quantization condition, $\gamma_{23}(\phi = 2\pi)$ is nearing π from below for $q = 0.1, 0.2, 0.3 \text{ \AA}$. At $q = 0.4, 0.6 \text{ \AA}$, $\gamma_{23}(\phi = 2\pi)$ is practically equal to π . In fact, if we look closely at the plots of ADT angle, the value of $\gamma_{23}(\phi = 2\pi)$ increases slightly as q increases. Here also, the 2- and 3-state calculations for ADT angle are giving almost similar results. We can further improve the $\gamma_{23}(\phi = 2\pi)$ value for $q = 0.1, 0.2, 0.3 \text{ \AA}$ if we consider neighboring electronic states in calculations.

For $q = 1.0, 1.2, 1.8 \text{ \AA}$ (Figures 2.20, 2.21, 2.22), the coupling between $2^2A'$ and $3^2A'$ is significant as is evident from the NACT plots. As far as the quantization condition is concerned, $\gamma_{23}(\phi = 2\pi)$ is reaching π for 3-state calculation for $q = 1.0 \text{ \AA}$. For $q = 1.2 \text{ \AA}$, $\gamma_{23}(\phi = 2\pi)$ by 2-state equation is less than π but for 3-state, it is reaching above π . And for $q = 1.8 \text{ \AA}$, $\gamma_{23}(\phi = 2\pi)$ is greater than π for both 2- and 3-state calculations. Even when the radius of the loop is large, the (2,3) coupling has not diminished much. We would like to do calculations for more q values and also improve the obtained results so that we can get $\gamma_{23}(\phi = 2\pi)$ converge to π .

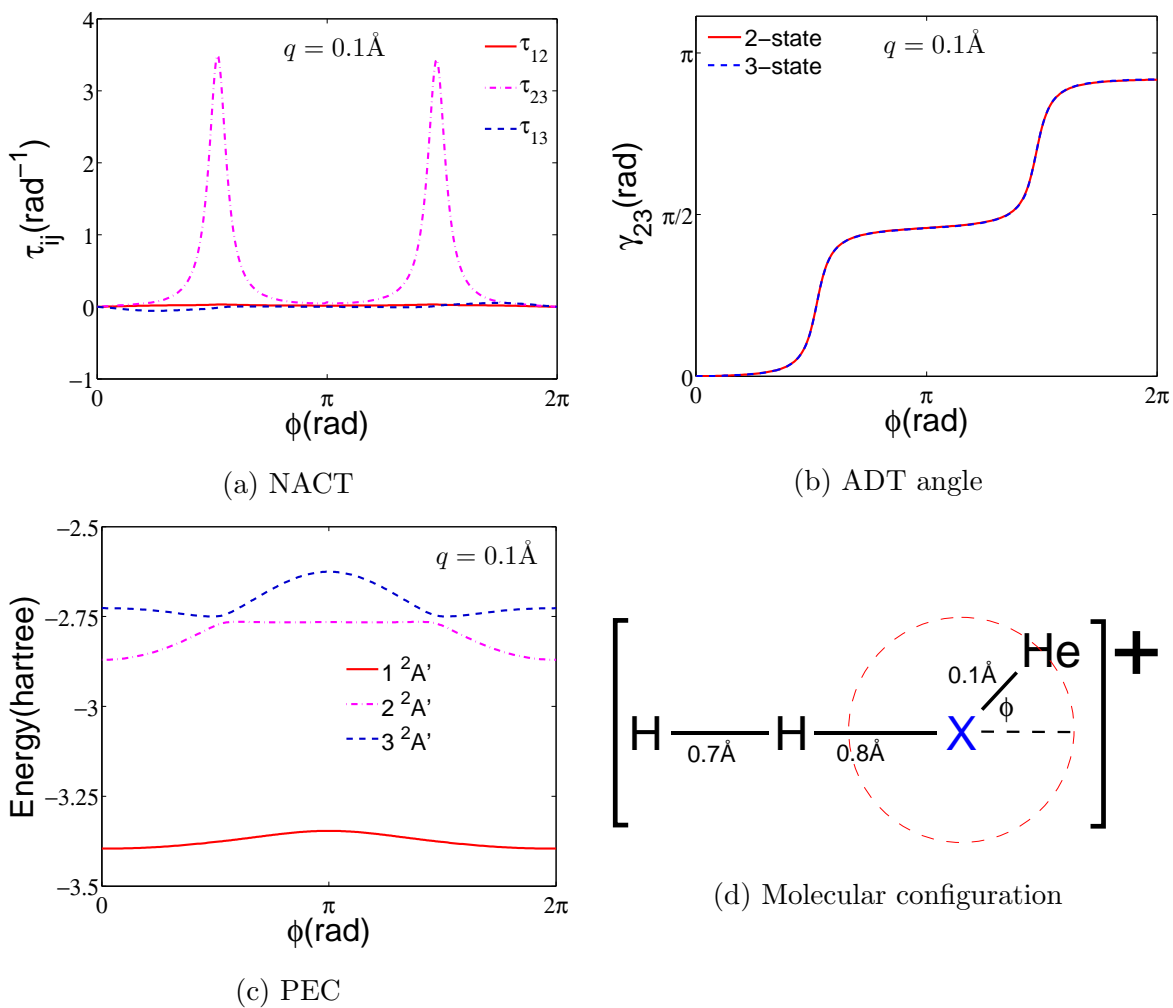


Figure 2.15: Plots of NACTs, ADT angle, and energy as a function of ϕ for $q = 0.1\text{\AA}$ of Scheme-2

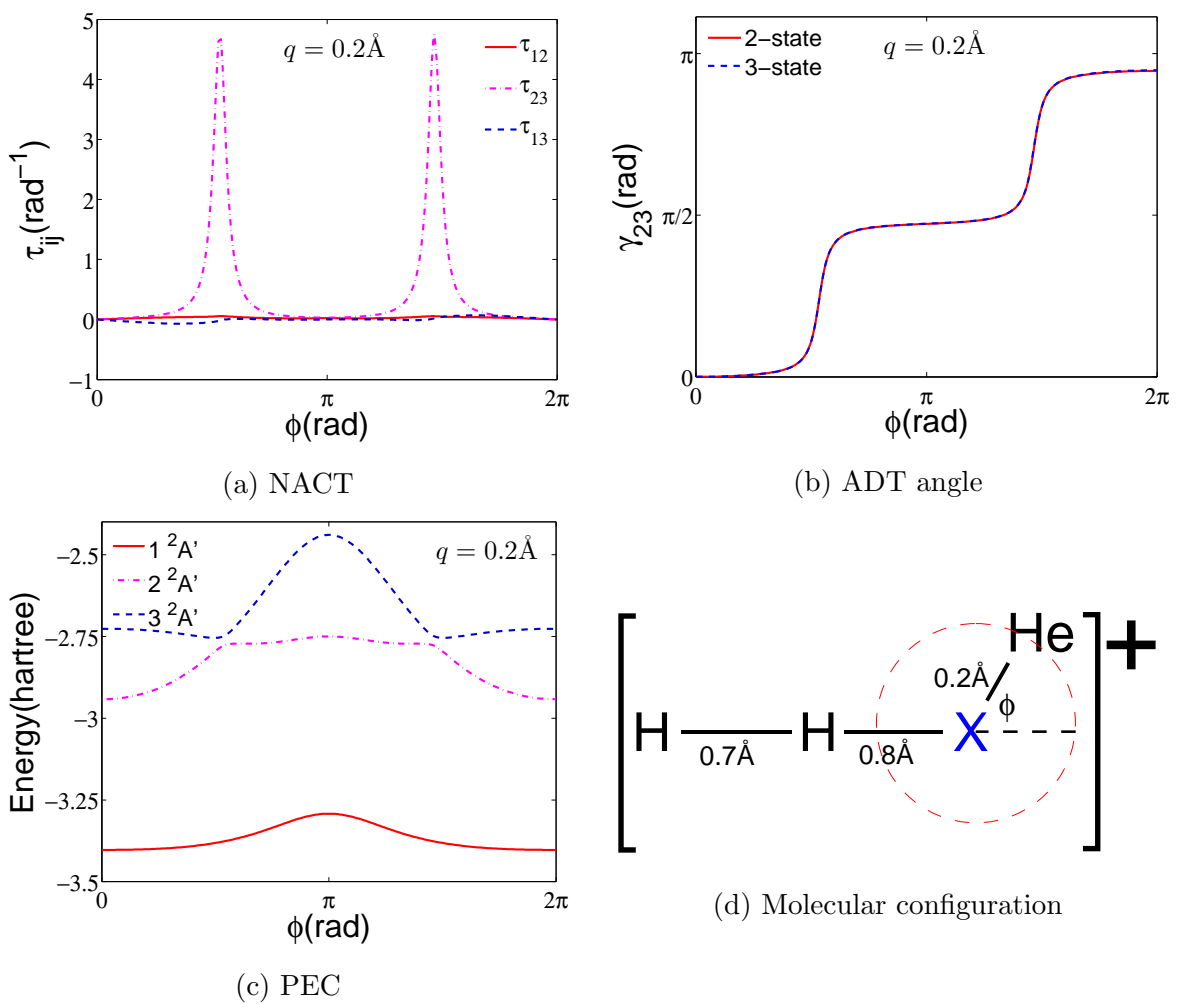


Figure 2.16: Plots of NACTs, ADT angle, and energy as a function of ϕ for $q = 0.2\text{\AA}$ of Scheme-2

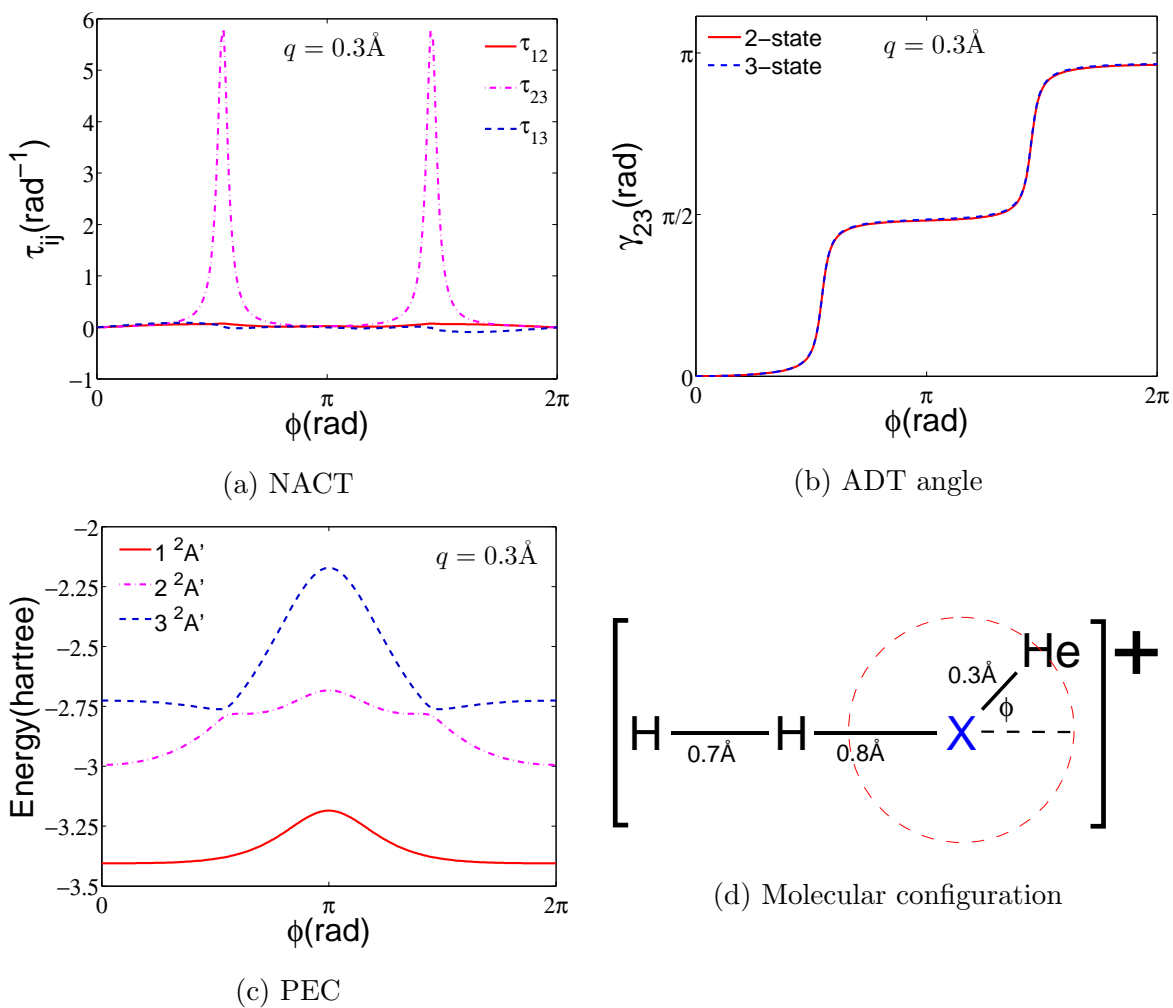


Figure 2.17: Plots of NACTs, ADT angle, and energy as a function of ϕ for $q = 0.3\text{\AA}$ of Scheme-2

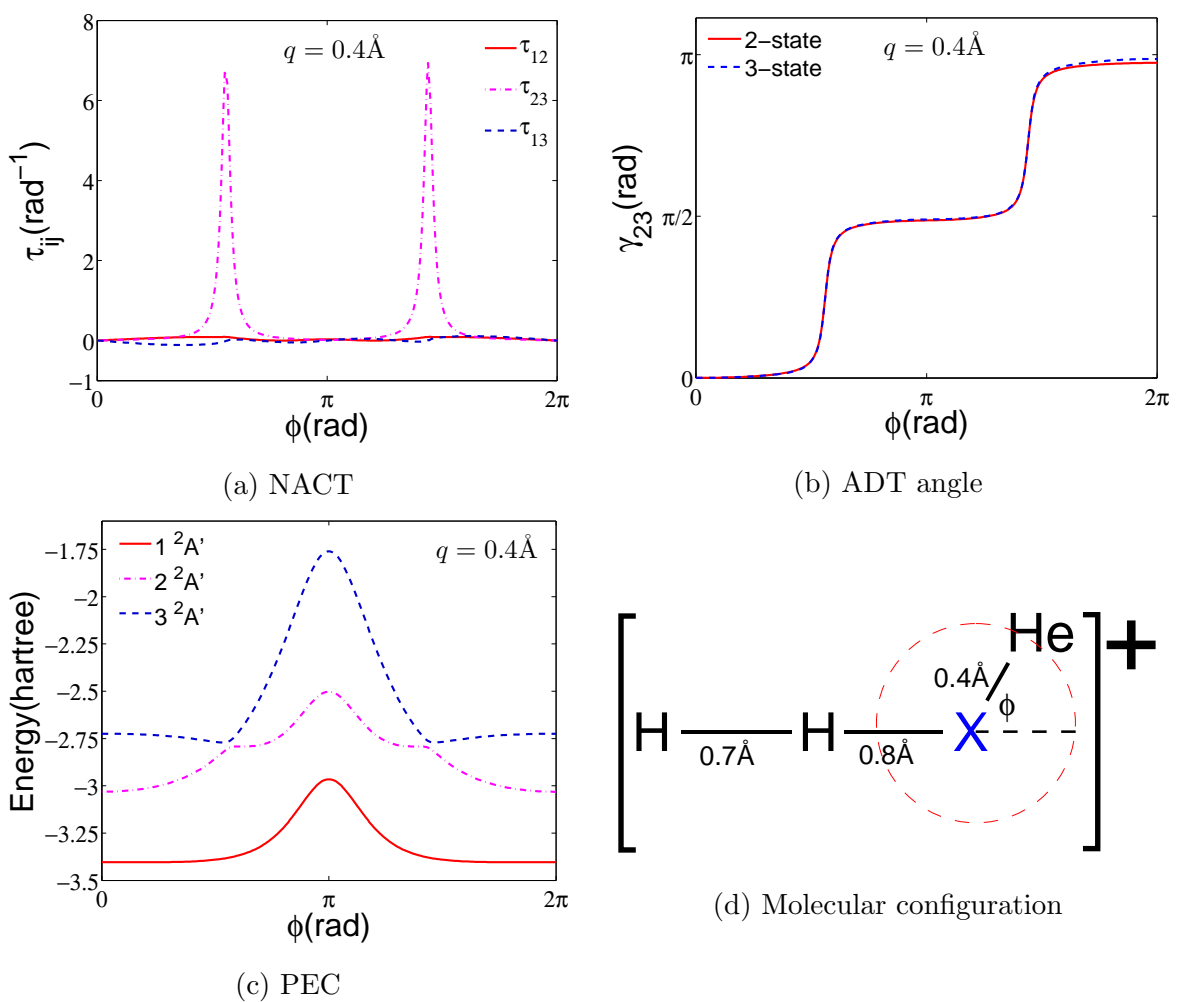


Figure 2.18: Plots of NACTs, ADT angle, and energy as a function of ϕ for $q = 0.4\text{\AA}$ of Scheme-2

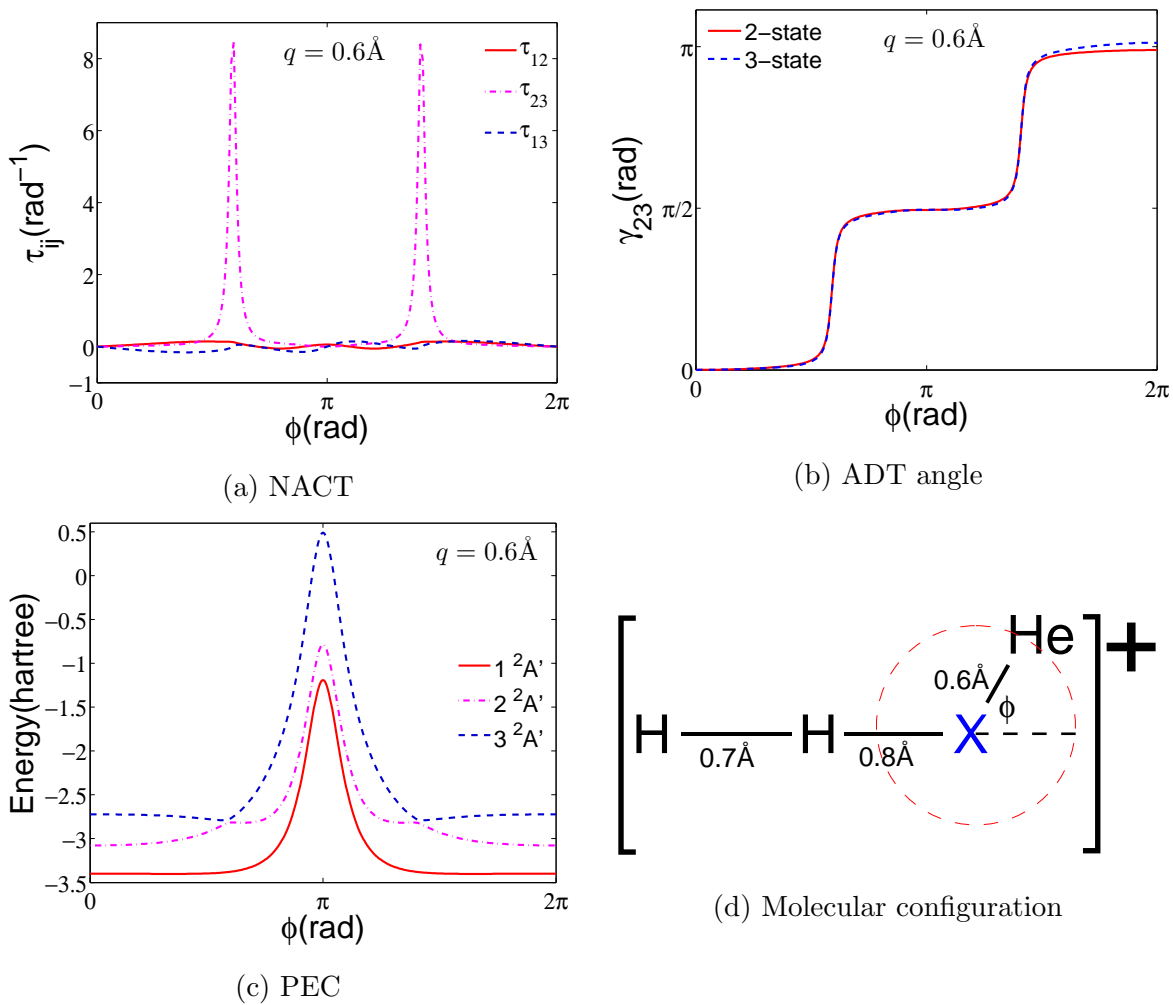


Figure 2.19: Plots of NACTs, ADT angle, and energy as a function of ϕ for $q = 0.6\text{\AA}$ of Scheme-2

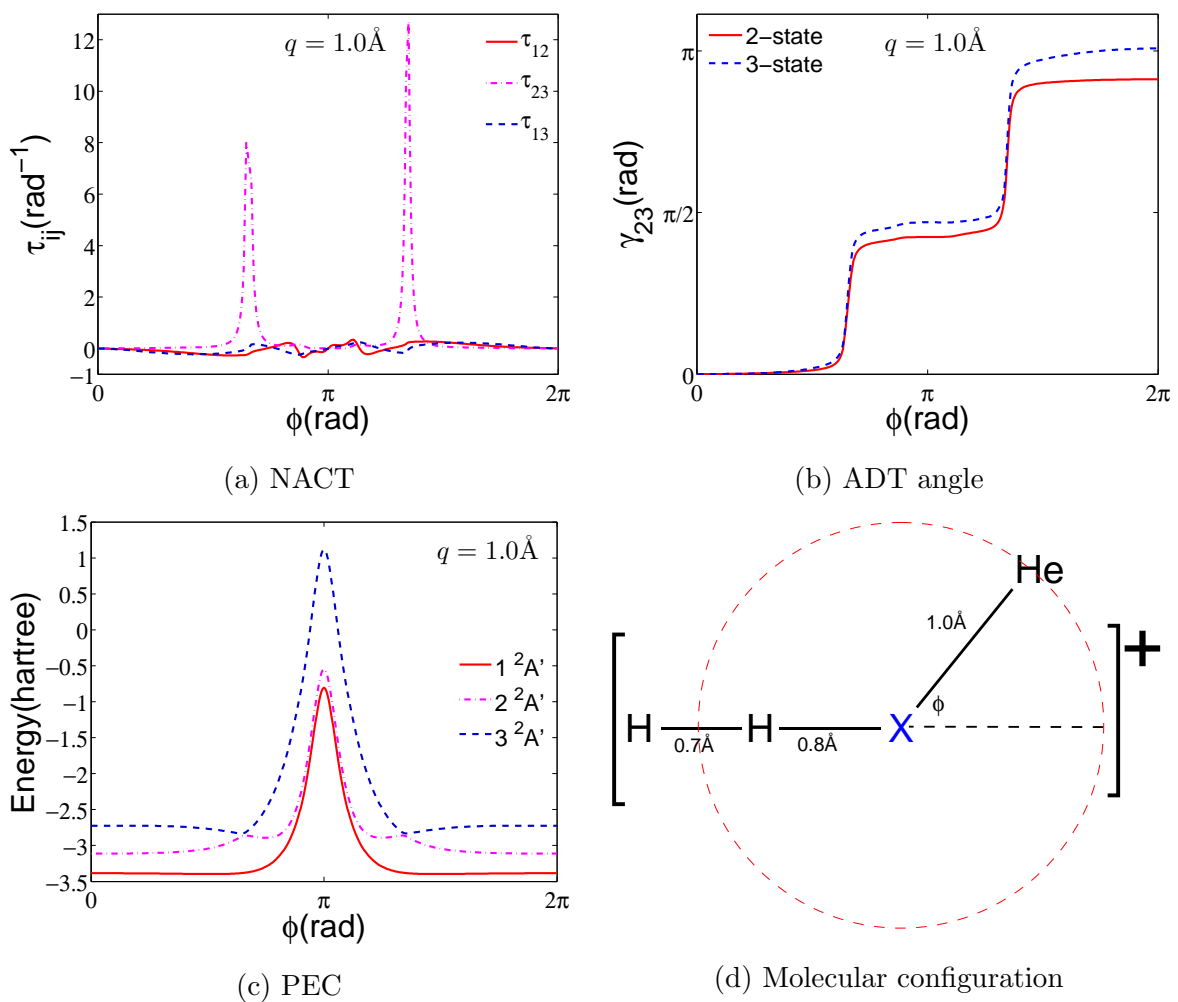


Figure 2.20: Plots of NACTs, ADT angle, and energy as a function of ϕ for $q = 1.0\text{\AA}$ of Scheme-2

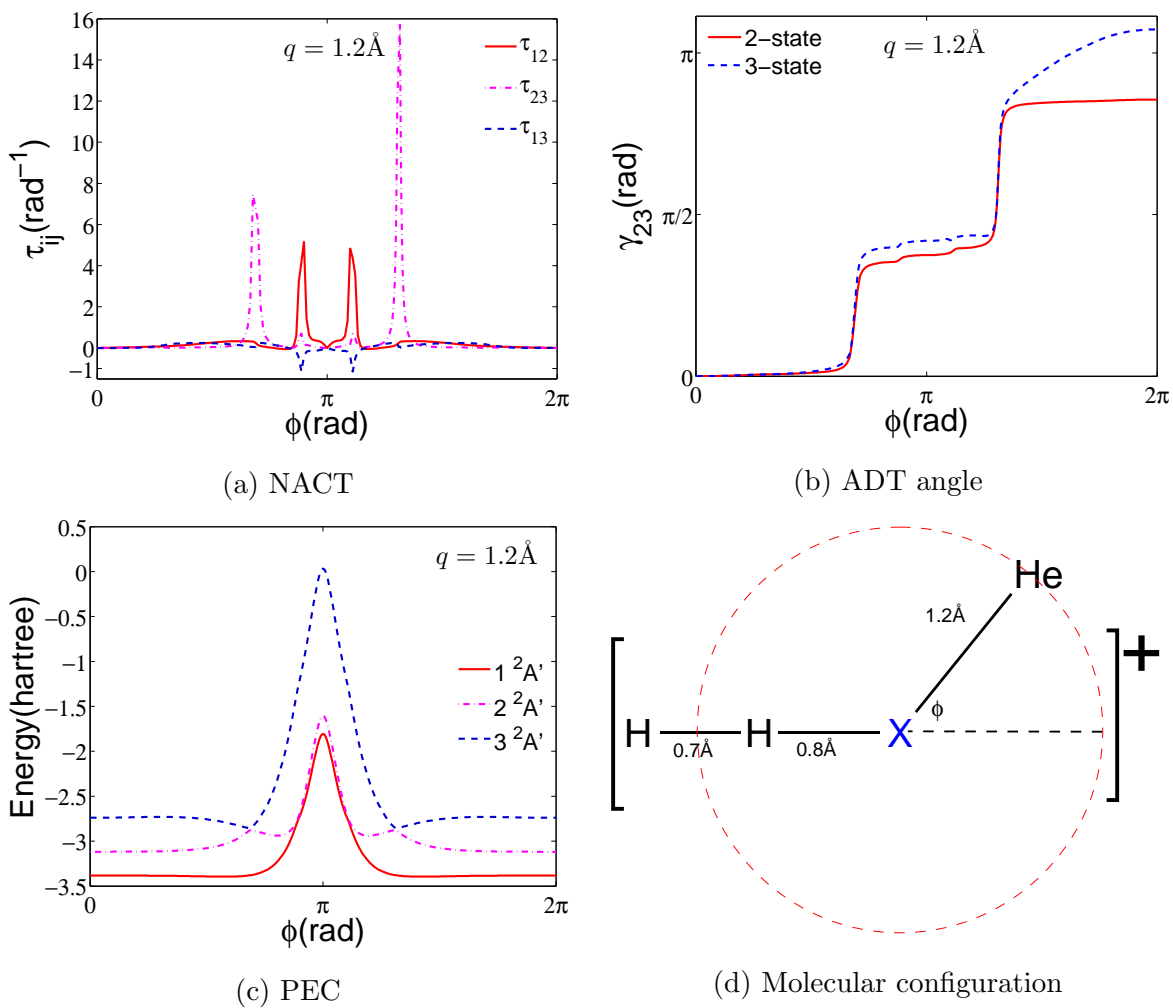


Figure 2.21: Plots of NACTs, ADT angle, and energy as a function of ϕ for $q = 1.2\text{\AA}$ of Scheme-2

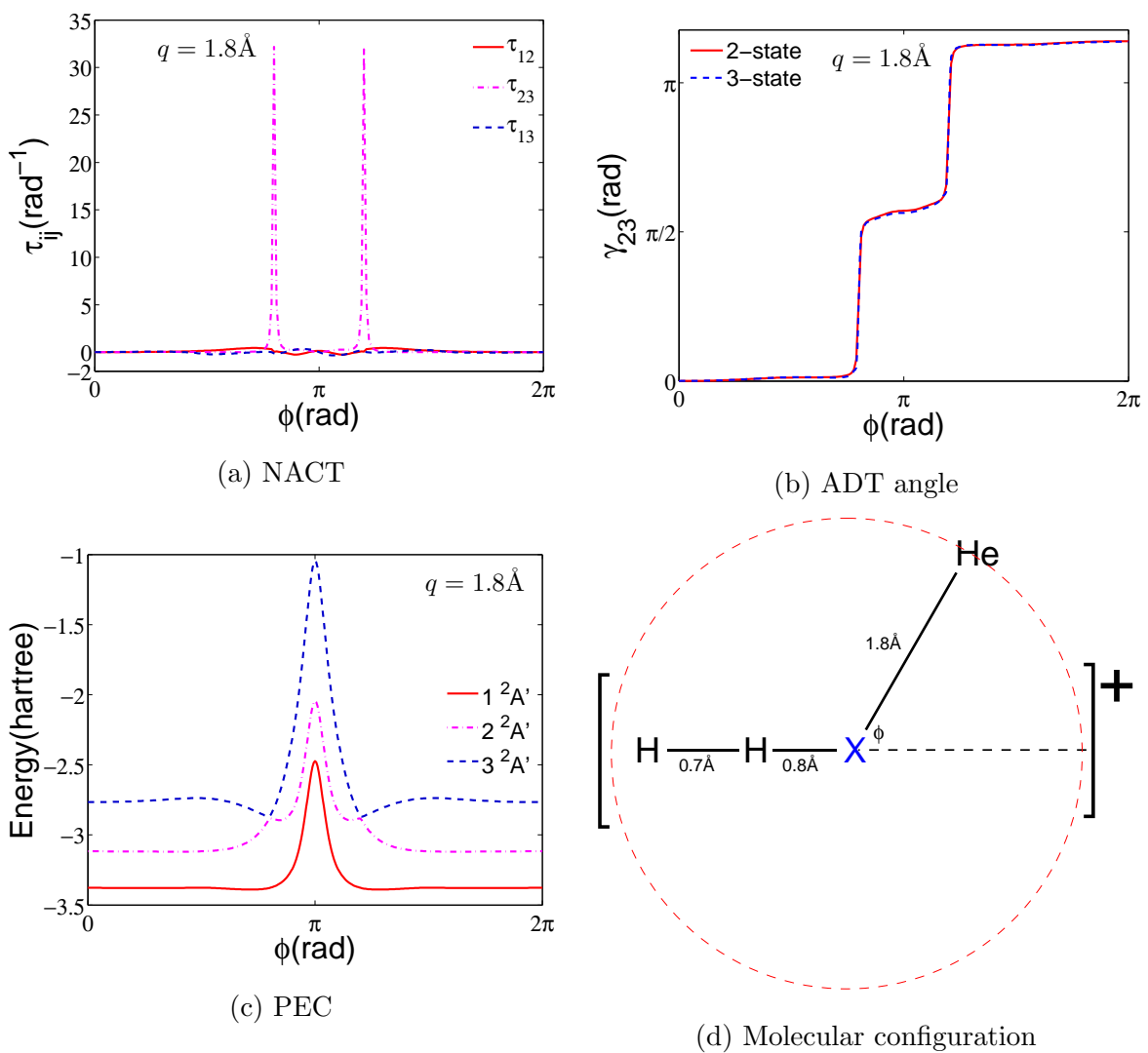


Figure 2.22: Plots of NACTs, ADT angle, and energy as a function of ϕ for $q = 1.8\text{\AA}$ of Scheme-2

2.3 Non-linear HHeH⁺

While plotting PECs for HeH₂⁺ for various geometries, we found a another nuclear configuration for which a point of degeneracy between the ground state and the first excited state was observed. But we detected it for a non-linear geometry and also the nuclear arrangement was a bit different. In this section, we will show calculations and observations for the CI between the ground state and the first excited state for non-linear HHeH⁺. The molecular geometry which we are considering is shown in Figure 2.23.

We plotted the 3-D PES diagram for the lowest three doublet states for HHeH⁺ (Figure 2.24). For the 3-D plot, the x-axis, y-axis, and z-axis were chosen to be the H-He bond length (Å), He-H bond length (Å), and the potential energy (Hartree) of the molecule as a function of these bond distances, respectively. Here since the point group of the non-linear HHeH⁺ is taken to be C_s , the three states have been assigned as $^2A'$. From Figure 2.24, it is clear that the two lowest excited states are significantly apart while the lowest two states are approaching close to each other for a certain nuclear coordinate zone. To distinctly make out the CI between the two lowest states, we have amplified the zone close to CI (Figure 2.25). Figure 2.25 clearly shows the CI between the ground state ($1^2A'$) and the first excited state ($2^2A'$). From the data, the molecular geometry at which the PESs are closest to each other was found to be $R(\text{H-He})= 1.0\text{Å}$ and $R(\text{He-H})= 1.0\text{Å}$.

Following the same procedure to proceed with the calculation for the confirmation of CI as explained in section 2.2, we obtain the molecular configuration for non-linear HHeH⁺ showing the closed around CI (Figure 2.26).

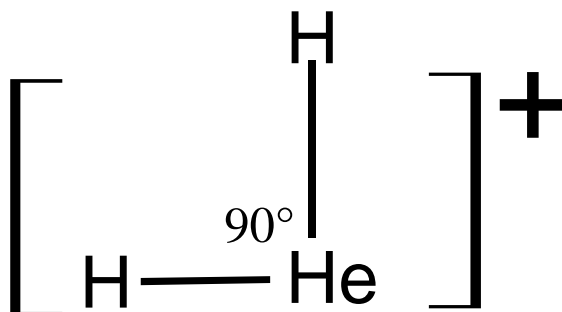


Figure 2.23: Non-linear HHeH⁺ molecule

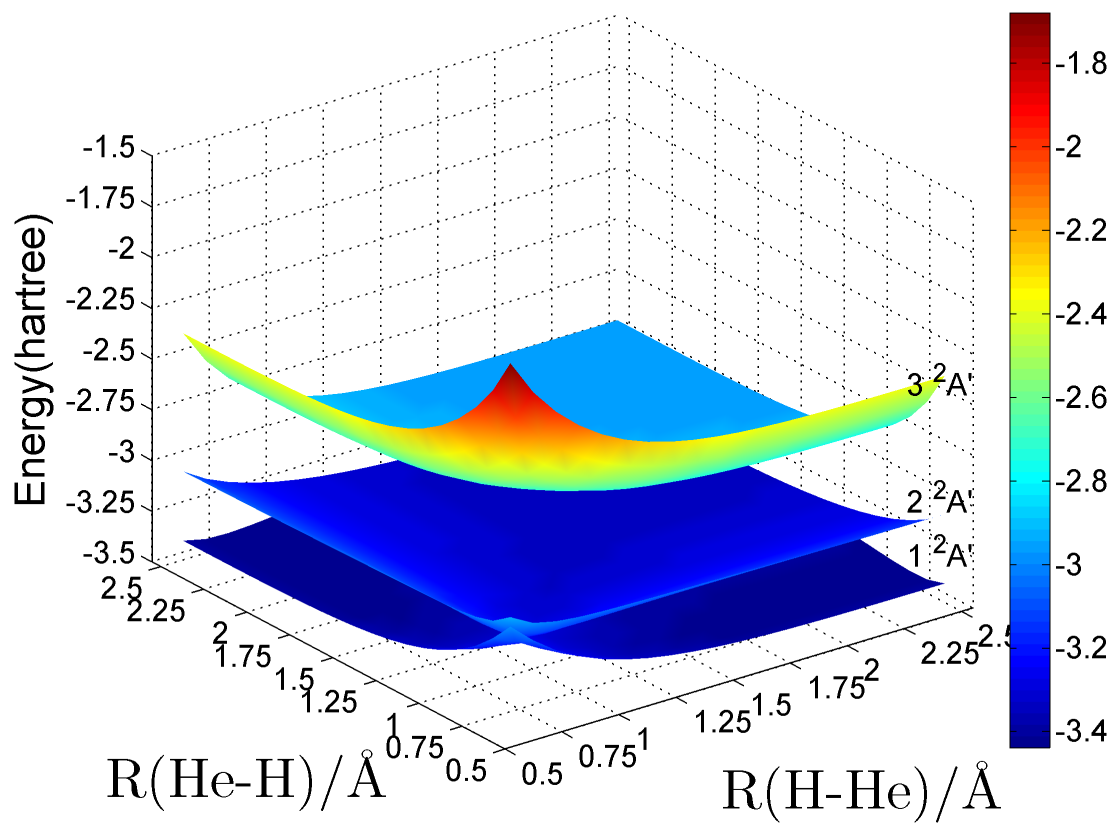


Figure 2.24: PES diagram depicting lowest three states for non-linear HHeH⁺

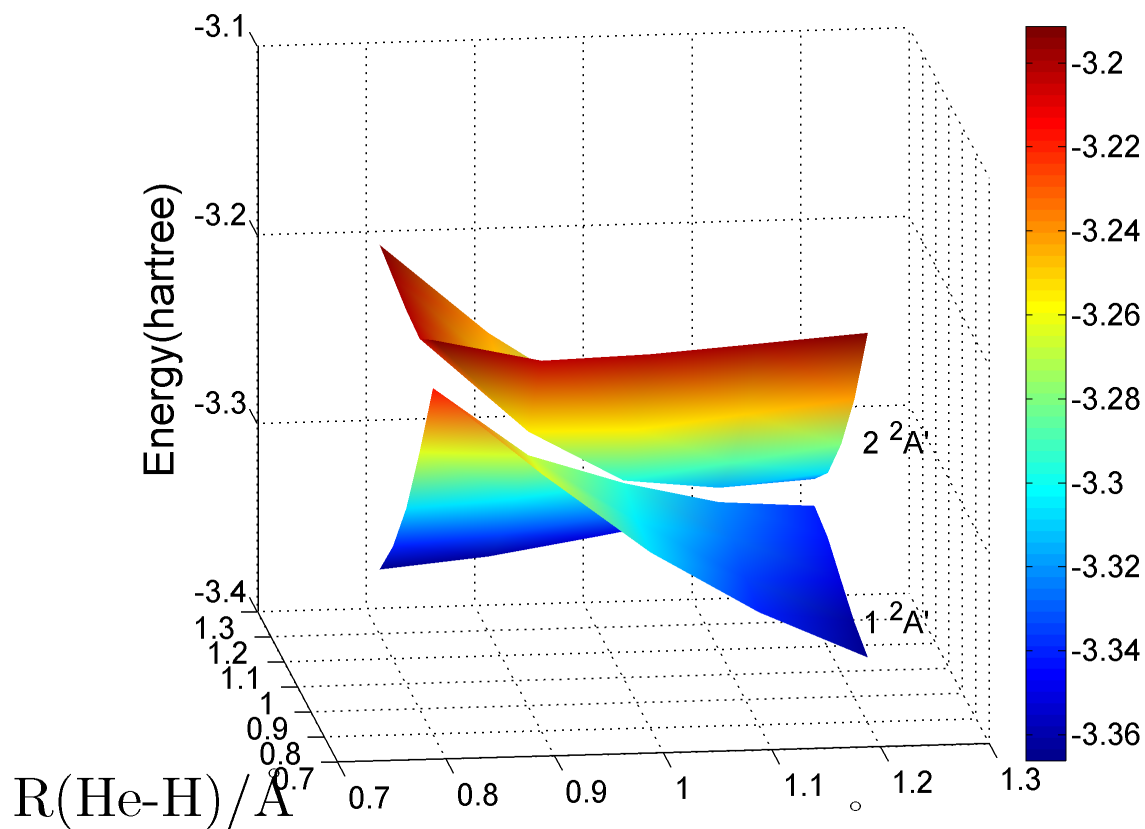


Figure 2.25: Close-up view of the region where the PESs of the two lowest electronic states are close to each other (for non-linear HHeH⁺)

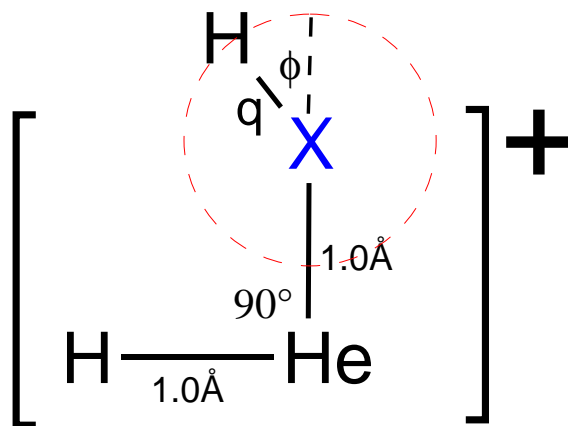


Figure 2.26: Molecular configuration of HHeH⁺ used to calculate NACTs and ADT angle

Since we found a CI between the ground state and the first excited state, we have to do calculations for (1,2) CI. Therefore, we are calculating γ_{12} as a function of ϕ and the corresponding quantization condition is,

$$\gamma_{12}(\phi = 2\pi) = \alpha_{12} = \pi \quad (2.7)$$

where α_{12} is the corresponding geometrical phase. We have to calculate $\gamma_{12}(\phi)$ using both 2- and 3-state methods (equations (2.2) and (2.3)).

We calculated NACTs ($\tau_{12}, \tau_{23}, \tau_{13}$ representing the coupling between the lowest three states), ADT angle (γ_{12}) using both 2-state and 3-state methods, and energy as a function of ϕ for different q values for the molecular configuration shown in Figure 2.26. We did calculations for $q = 0.1, 0.2, 0.3, 0.4, 0.6, 0.8, 1.2, 1.6, 2.0 \text{ \AA}$.

For $q = \mathbf{0.1, 0.2 \text{ \AA}}$ (Figures 2.28, 2.29), the results are along the expected lines. We can see a strong coupling between $1^2A'$ and $2^2A'$ from the NACT plots. PEC diagrams show this as well. $\gamma_{12}(\phi = 2\pi)$ is reaching π for both 2- and 3-state calculations. In fact, $\gamma_{12}(\phi = 2\pi)$ is exactly equal to π for $q = 0.1 \text{ \AA}$.

Unfortunately, the results are not very encouraging for $q = \mathbf{0.3, 0.4, 0.6, 0.8 \text{ \AA}}$ (Figures 2.30, 2.31, 2.32, 2.33). The coupling between the lowest two states (τ_{12}) decreased significantly for the given q values. As a result, $\gamma_{12}(\phi = 2\pi)$ is not even reaching $\pi/2$. The closed contour is definitely enclosing the CI but the calculations are not in agreement with the theory. Maybe we will have to redo the calculations including other excited electronic states.

For $q = \mathbf{1.2, 1.6 \text{ \AA}}$ (Figures 2.34, 2.35), instead of (1,2) coupling (τ_{12}), (2,3) coupling (τ_{23}) is significantly larger than the others. This is not very surprising because we are considering such a large loop and it is possible that the two excited states are close to each other (maybe even intersecting) in that region. As far as the quantization condition is concerned, 3-state calculations show some promise. Although, $\gamma_{12}(\phi = 2\pi)$ is not reaching π , but the results can be improved in this case.

Finally we are considering $q = \mathbf{2.0 \text{ \AA}}$ (Figure 2.36). As stated earlier, from the PES diagram (Figure 2.24) we found the molecular geometry at which $1^2A'$ and $2^2A'$ are forming a CI and that is $R(\text{H-He}) = 1.0 \text{ \AA}$ and $R(\text{He-H}) = 1.0 \text{ \AA}$. But since non-linear $[\text{H-He-H}]^+$ is a symmetric molecule, we have two equivalent configurations at which we would observe a CI (Figure 2.27). Although these two configurations are same in every respect, yet when we move along the closed contour for $q = 2.0 \text{ \AA}$ (Figure 2.36d), we will encounter Configuration-2 (Figure 2.27b) at $\phi = \pi$ and we will observe a CI between $1^2A'$ and $2^2A'$ at that geometry which is apparent from Figure 2.36c. The magnitude of τ_{12} coupling is

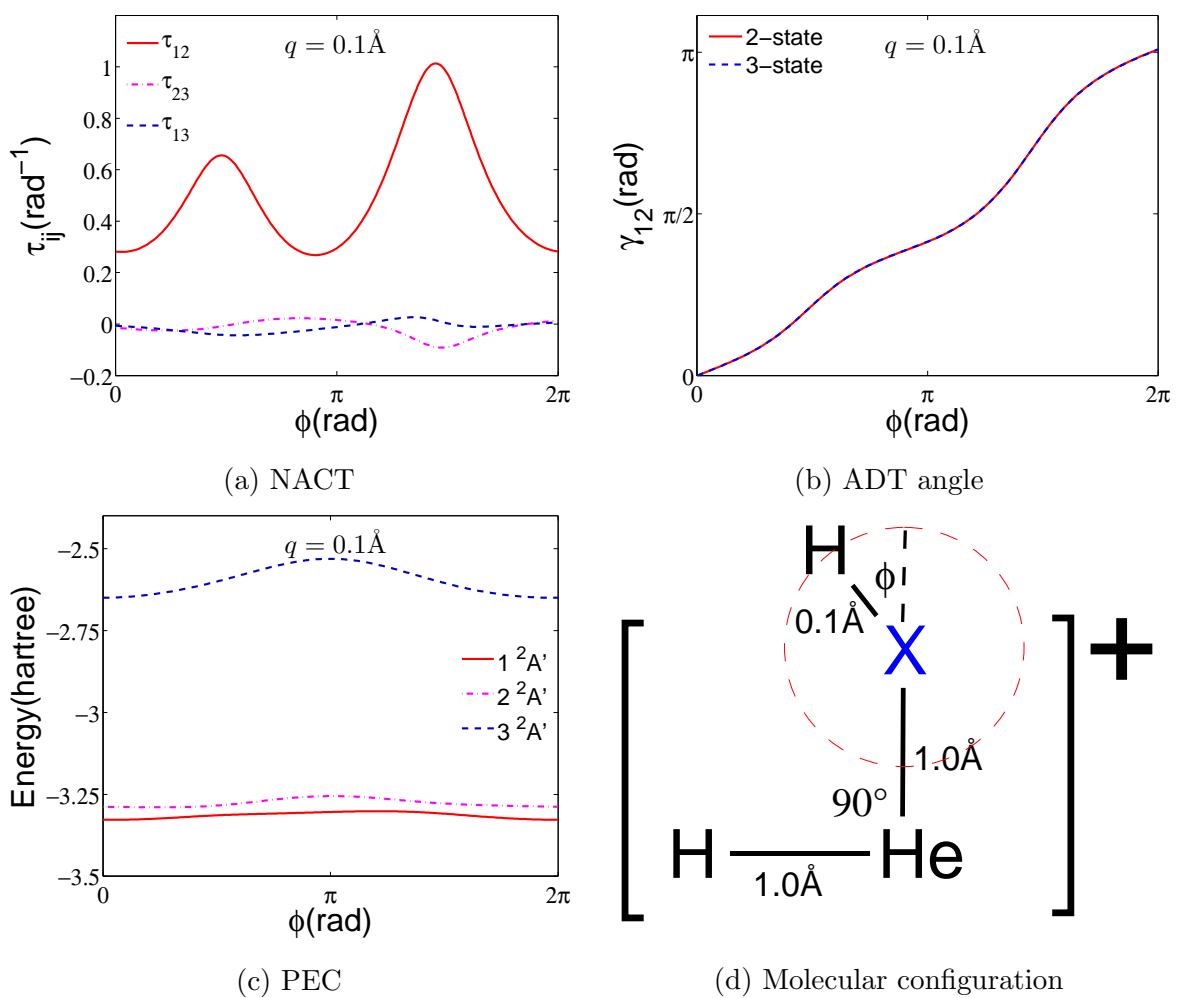


Figure 2.28: Plots of NACTs, ADT angle, and energy as a function of ϕ for $q = 0.1 \text{ \AA}$ for non-linear HHeH^+

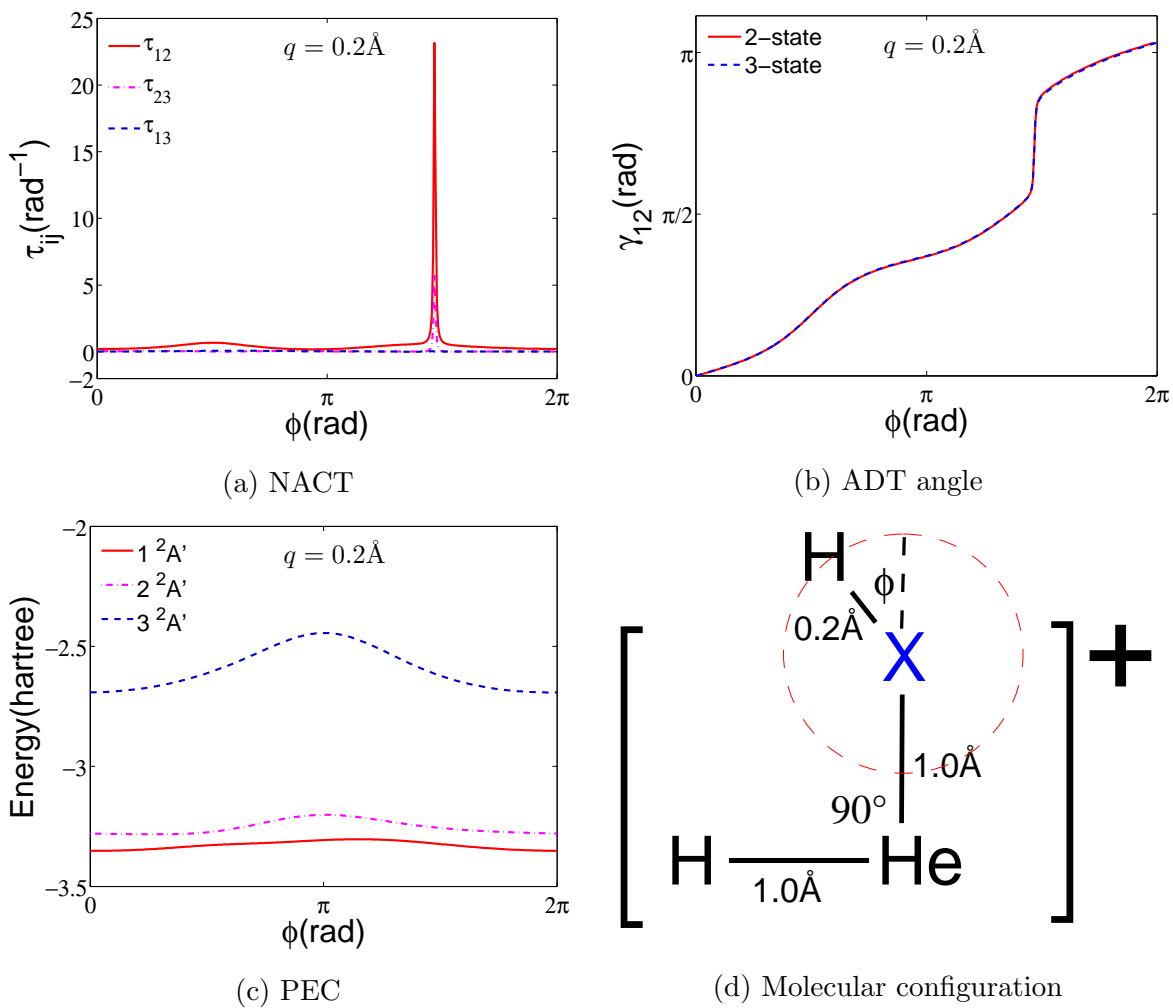


Figure 2.29: Plots of NACTs, ADT angle, and energy as a function of ϕ for $q = 0.2\text{\AA}$ for non-linear HHeH^+

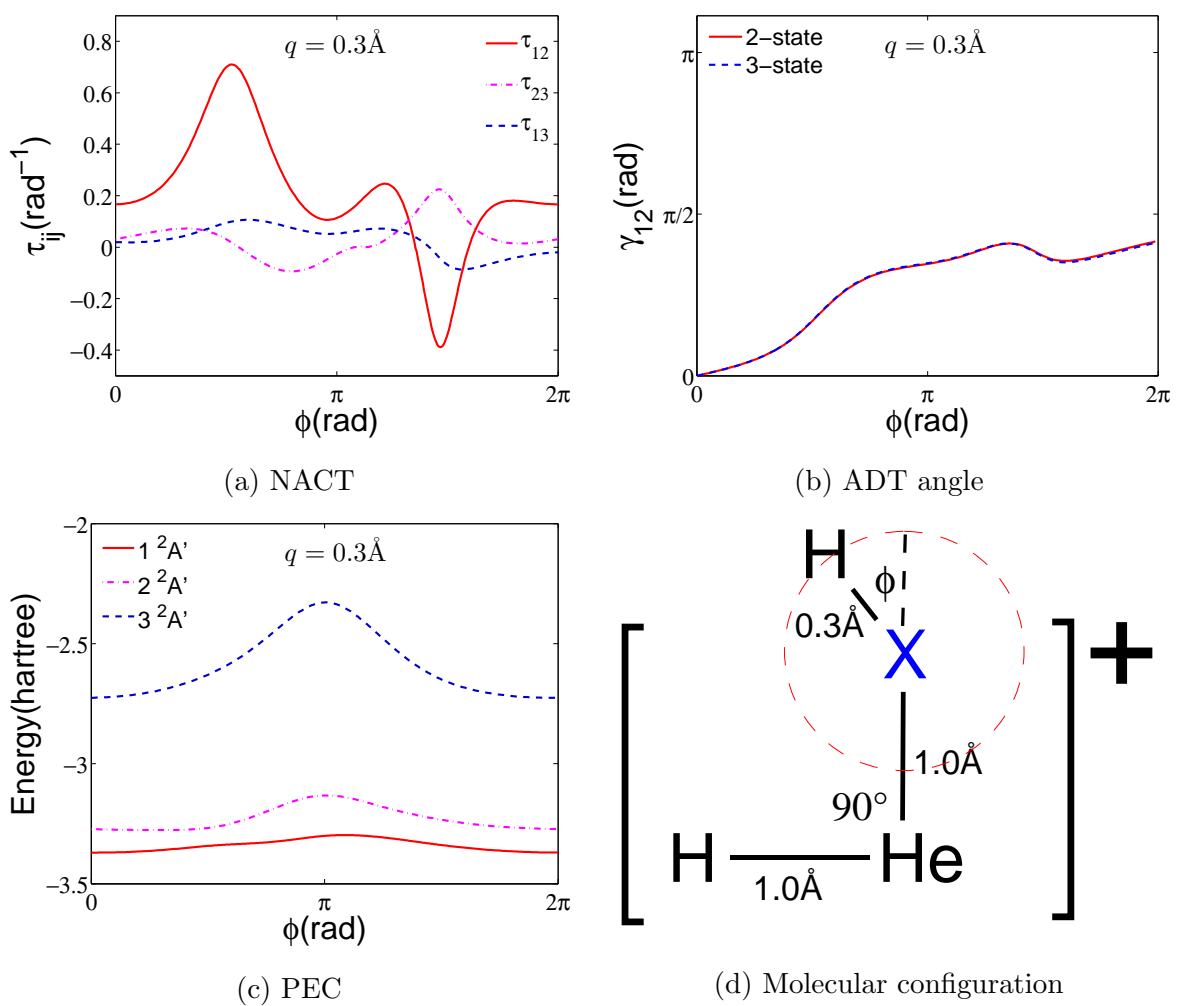


Figure 2.30: Plots of NACTs, ADT angle, and energy as a function of ϕ for $q = 0.3\text{\AA}$ for non-linear HHeH^+

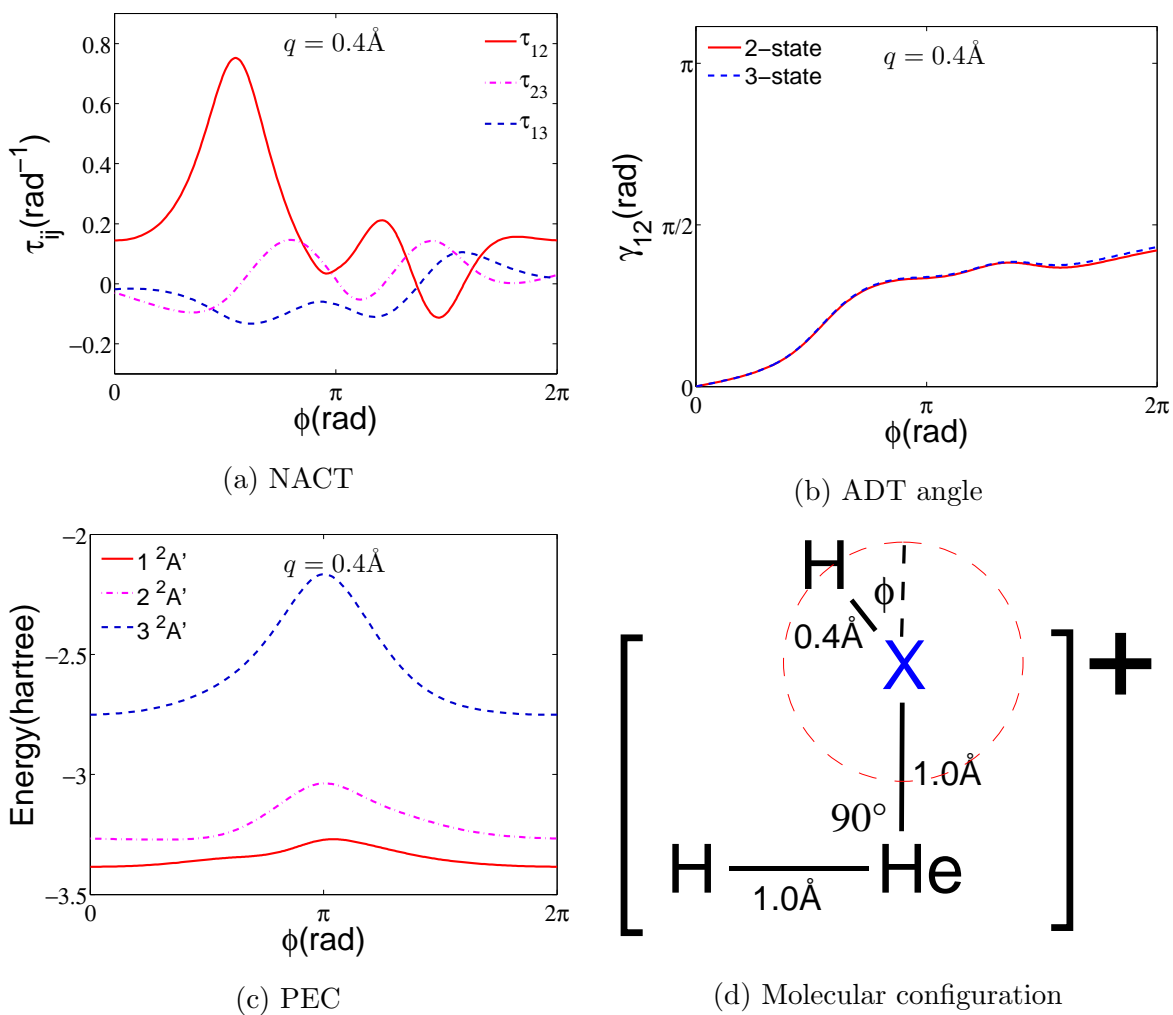


Figure 2.31: Plots of NACTs, ADT angle, and energy as a function of ϕ for $q = 0.4\text{\AA}$ for non-linear HHeH^+

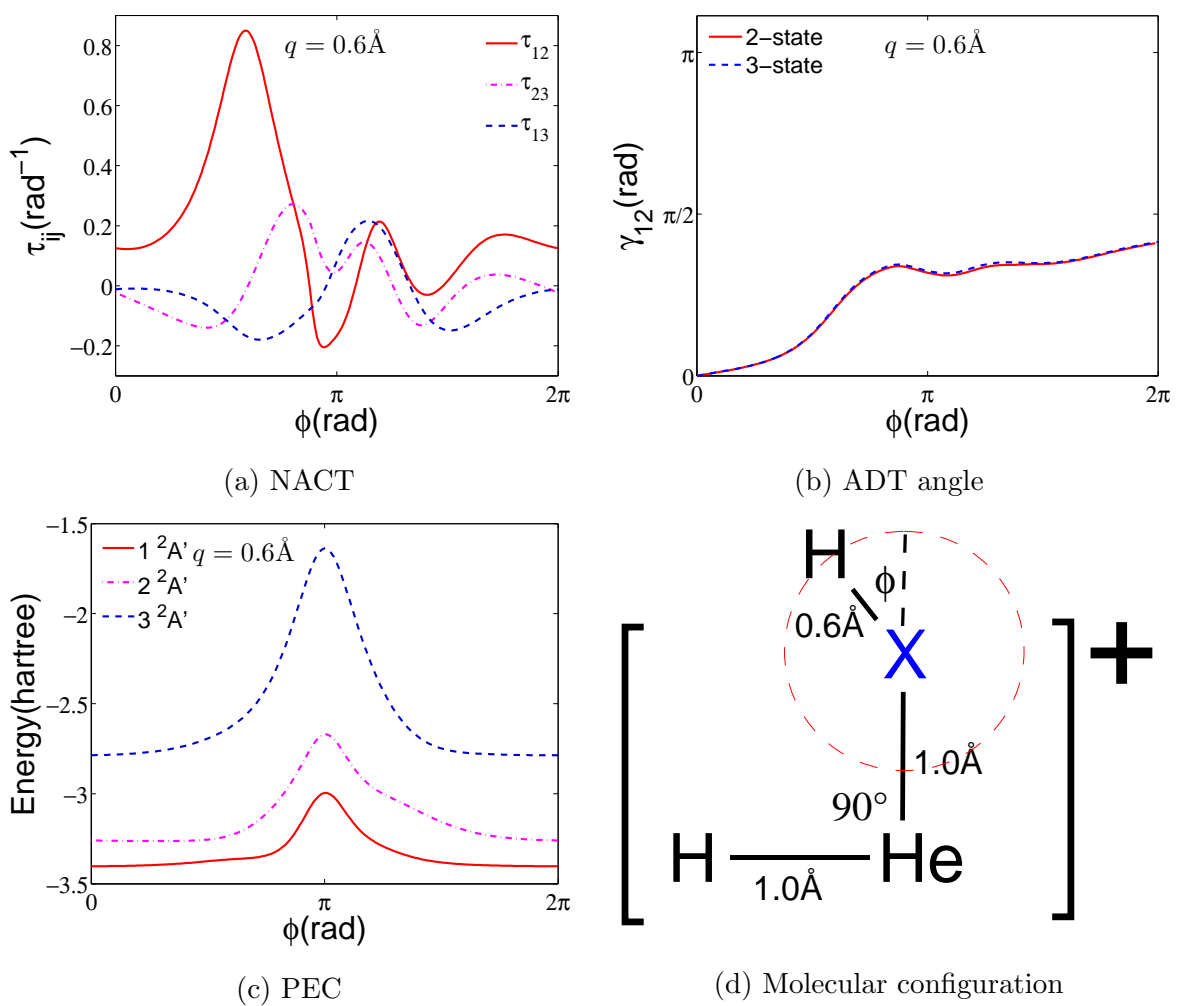
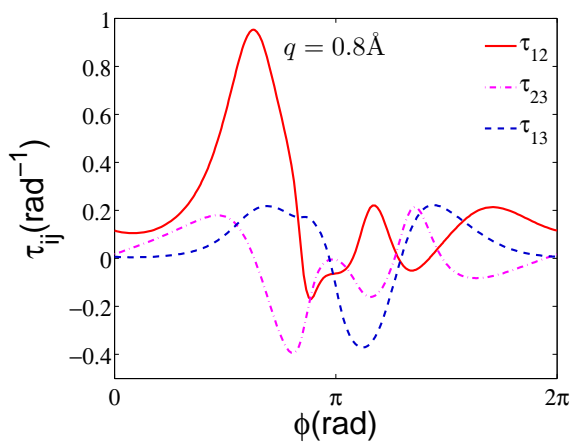
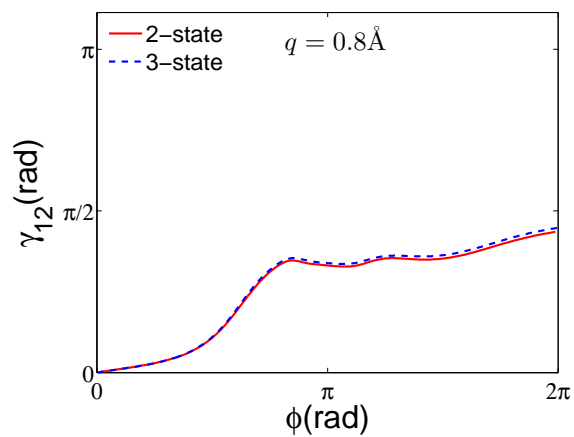


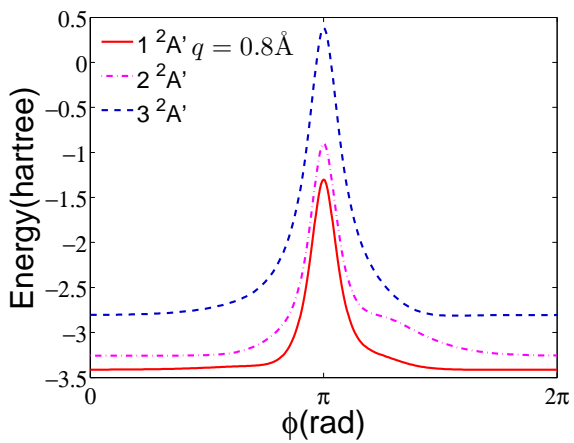
Figure 2.32: Plots of NACTs, ADT angle, and energy as a function of ϕ for $q = 0.6\text{\AA}$ for non-linear HHeH^+



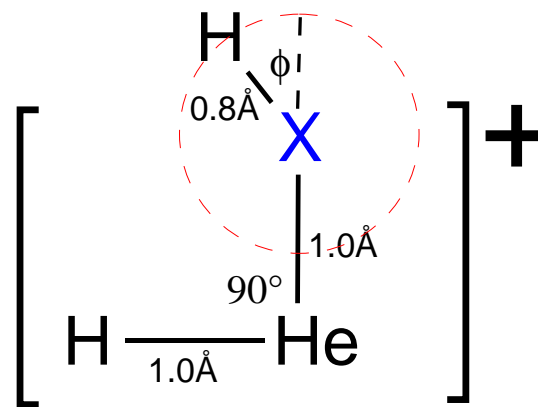
(a) NACT



(b) ADT angle



(c) PEC



(d) Molecular configuration

Figure 2.33: Plots of NACTs, ADT angle, and energy as a function of ϕ for $q = 0.8\text{\AA}$ for non-linear HHeH^+

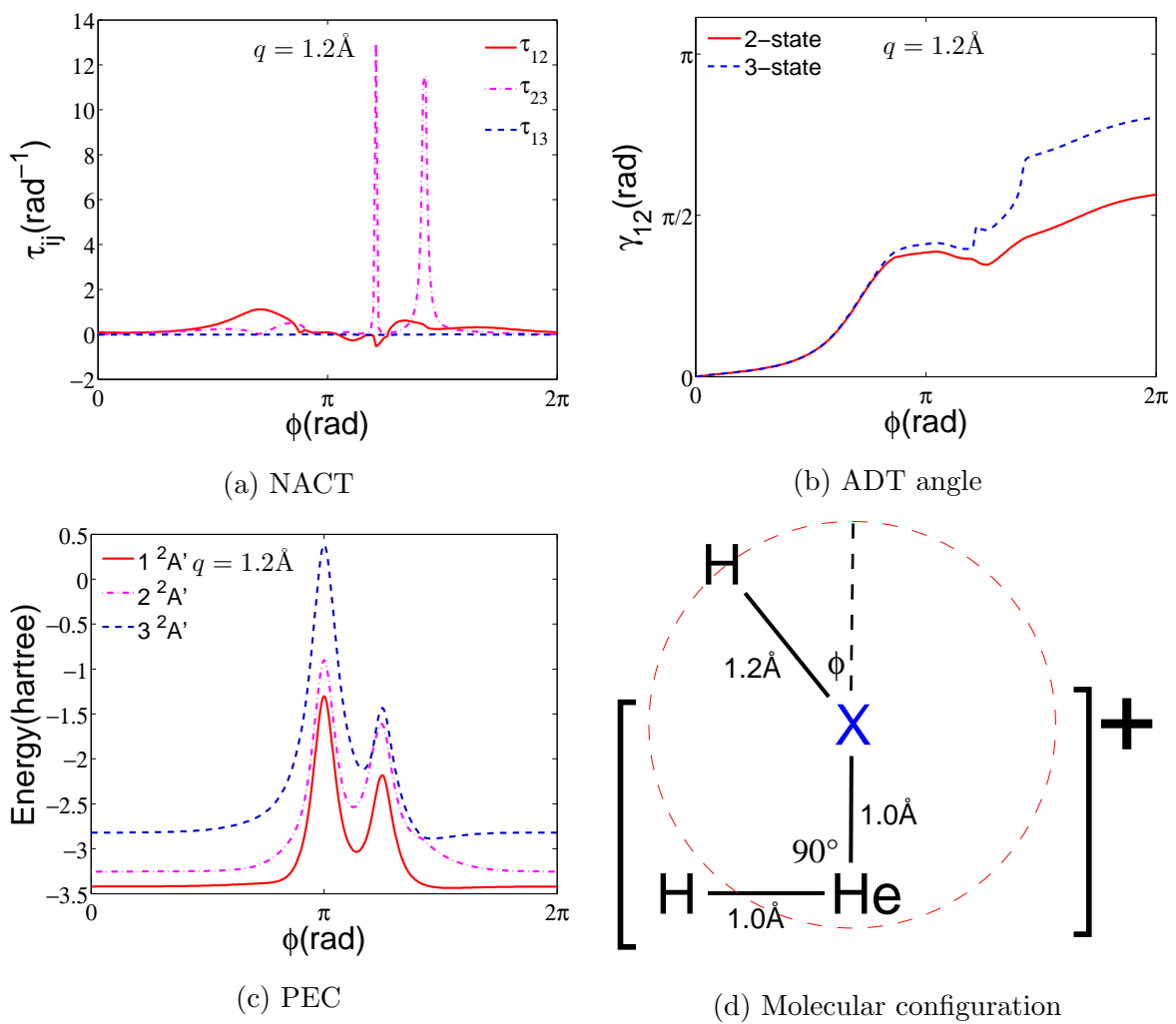


Figure 2.34: Plots of NACTs, ADT angle, and energy as a function of ϕ for $q = 1.2\text{\AA}$ for non-linear HHeH^+

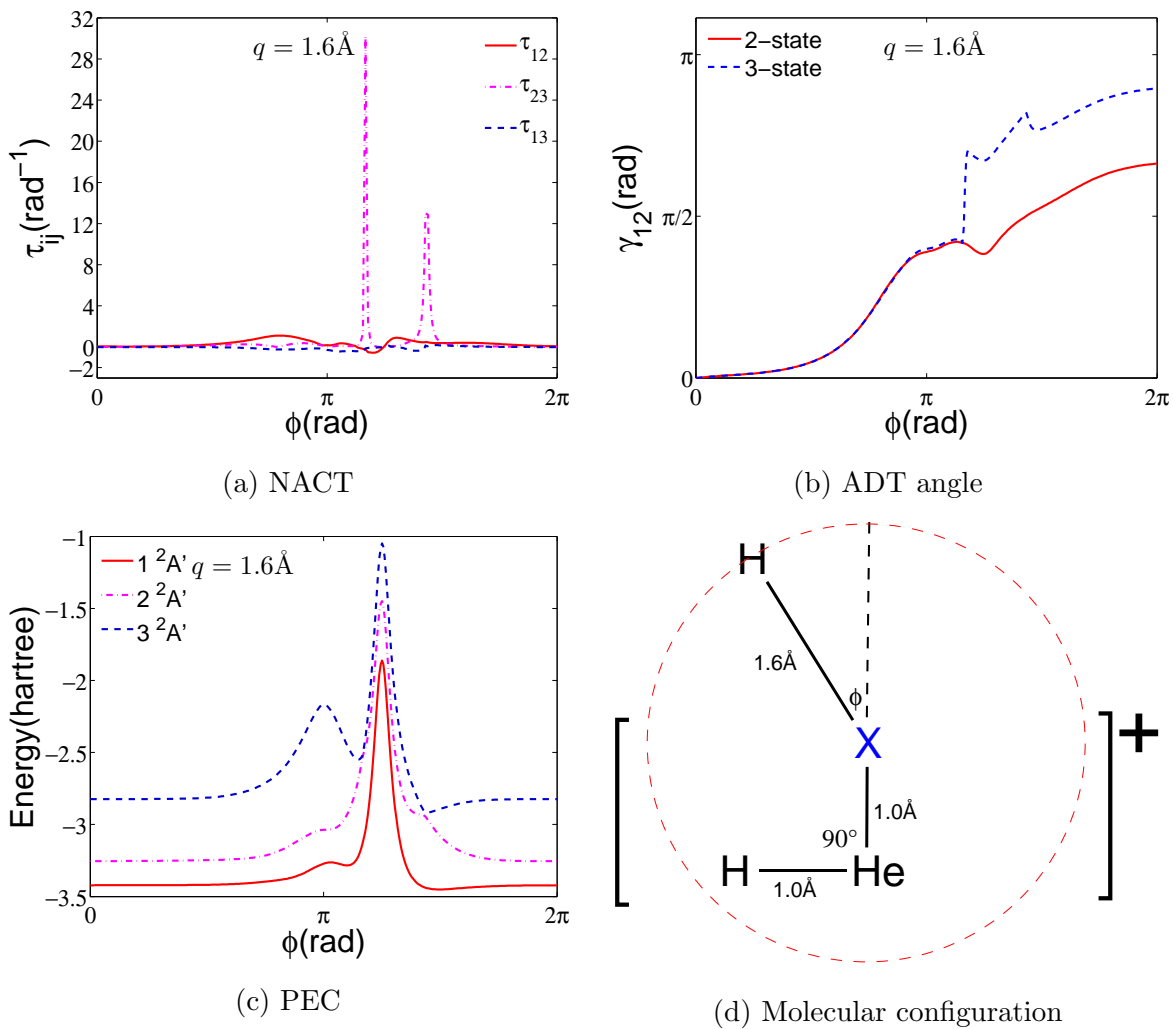


Figure 2.35: Plots of NACTs, ADT angle, and energy as a function of ϕ for $q = 1.6\text{\AA}$ for non-linear HHeH^+

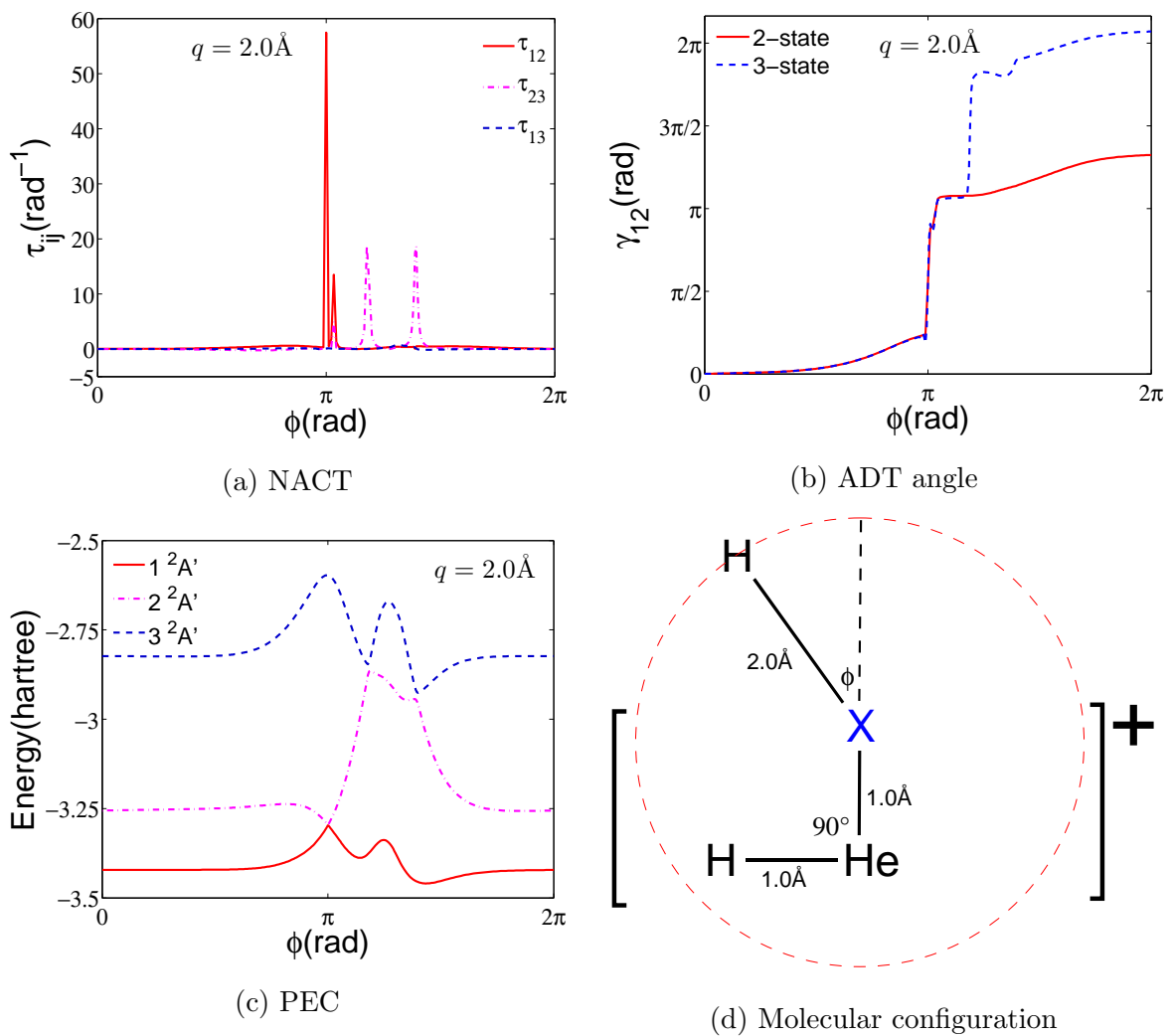


Figure 2.36: Plots of NACTs, ADT angle, and energy as a function of ϕ for $q = 2.0 \text{ \AA}$ for non-linear HHeH^+

2.4 Conclusion

It's always good to compare what the theory predicted and what results we got from practical calculations. In Chapter-1, we derived conditions to confirm the presence of CIs. One of the most important steps in the derivation, was the choice of the closed contour enclosing the CI (because of the *geometric phase effect* shown by electronic wavefunctions when a loop in nuclear coordinate space encloses a CI). Although, theoretically/from the theoretical derivation it is clear that the π -quantization condition will be satisfied as long as the closed contour encircles the CI (irrespective of the shape and size of the loop, and also the relative distance between the path of the contour and the CI), but can we say this based on the results that we have shown in Chapter-2? The answer is both yes and no. Some calculations indeed are in favor of the theory but then there are some which puts a question mark on the position of the closed contour relative to the CI. In other words, while some calculations indeed show π quantization, some of them do not!

For the linear HeH_2^+ , we could locate a CI between the second and the third electronic state ((2,3)CI)(Section 2.2) and did requisite calculations for it. For Scheme-1 (Section 2.2.1), the results are satisfactory for small q , but for $q \geq 1.0\text{\AA}$, the calculations are not in agreement with the theory. Whereas for Scheme-2 (Section 2.2.2), the results for both small and large q are almost satisfactory, but still more calculations are needed. Now, in any calculation (for CI), the most important step is the 3-state calculation for the ADT angle. For this, we included the ground state (as the 3rd state) in our calculations and got results. But one may wonder why didn't we consider the 4th electronic state (3rd excited state) for the 3-state calculations, since this state is also adjacent to (2,3)CI. In fact, this is our next step in order to solve the linear HeH_2^+ problem and get more accurate results. We would like to do 3-state calculations incorporating the lowest three excited states and also a 4-state calculation which will include the lowest four electronic states.

The results for non-linear HHeH^+ (Section 2.3) are interesting. In this case, we achieved the quantization condition for only three q values ($q = 0.1, 0.2, 2.0\text{\AA}$). And in all three cases, the path of the closed contour was *extremely close* to the molecular configuration representative of the concerned CI ((1,2)CI). While for other q values, the results are like that the CI has altogether vanished from the loop. Moreover, since we are studying the intersection between the lowest two electronic states, the inclusion of the 4th electronic state (which is energetically far from the lowest two states and hence from (1,2)CI) in the calculations may not have that much of an impact on the final result.

Bibliography

- [1] Chupka, W. A.; Russell, M. E.; Refaey, K. *J. Chem. Phys.* **1968**, *48*, 1518.
- [2] Kouri, D. J.; Baer, M. *Chem. Phys. Lett.* **1974**, *24*, 37.
- [3] Domcke, W., Yarkony, D. R., Köppel, H., Eds. *Conical Intersections: Electronic Structure, Dynamics & Spectroscopy*; Advanced Series in Physical Chemistry; World Scientific, 2004; Vol. 15.
- [4] Baer, M. *Beyond Born–Oppenheimer: Conical Intersections and Electronic Non-adiabatic Coupling Terms*; John Wiley & Sons: Hoboken, New Jersey, 2006.
- [5] Atkins, P.; Friedman, R. *Molecular Quantum Mechanics*, 4th ed.; Oxford University Press: Great Britain, 2005.
- [6] Köppel, H., Yarkony, D. R., Barentzen, H., Eds. *The Jahn-Teller Effect: Fundamentals and Implications for Physics and Chemistry*; Chemical Physics 97; Springer: Heidelberg, 2009.
- [7] Longuet-Higgins, H. C. *Proc. R. Soc. Lond.* **1975**, *A344*, 147–156.
- [8] Yarkony, D. R. *J. Phys. Chem.* **2001**, *105*, 6277–6293.
- [9] Levine, I. N. *Quantum Chemistry*, 6th ed.; Pearson Education: New Jersey, U.S.A., 2009.
- [10] Mead, C. A. *J. Chem. Phys.* **1979**, *70*, 2276.
- [11] Yarkony, D. R. *Chem. Rev.* **2012**, *112*, 481–498.
- [12] Bersuker, I. B. *The Jahn-Teller Effect*; Cambridge University Press: U.K., 2006.
- [13] Yarkony, D. R. *Acc. Chem. Res.* **1998**, *31*, 511–518.

- [14] Werner, H. J.; Knowles, P. J.; Knizia, G.; Manby, F. R.; Schütz, M. MOLPRO, version 2012.1, a package of ab initio programs. 2012.
- [15] Alijah, A.; Baer, M. *J. Phys. Chem.* **2004**, *104*, 389–396.